Journal of Archaeological Science 117 (2020) 105121

Contents lists available at ScienceDirect

Journal of Archaeological Science

journal homepage: http://www.elsevier.com/locate/jas

Research Papers

An archaeological strontium isoscape for the prehistoric andes: Understanding population mobility through a geostatistical meta-analysis of archaeological $^{87}Sr/^{86}Sr$ values from humans, animals, and artifacts

Beth K. Scaffidi [a,*], Kelly J. Knudson [a]

[a] Center for Bioarchaeological Research, School of Human Evolution and Social Change, Arizona State University, 900 Cady Mall, Tempe, AZ, 85287-2402, USA

ARTICLE INFO

Keywords:
Paleomobility
Migration
Bioarchaeology
Geostatistics
Geolocation/provenience

ABSTRACT

Biogeographical studies of migration and mobility in archaeology and bioarchaeology rely on accurately characterizing local $^{87}Sr/^{86}Sr$ ranges, either through baseline studies or by statistically parsing archaeological results at a given site. However, when baseline materials are difficult to obtain or suspected to deviate from prehistoric isotopic catchments, archaeological data may provide an accurate characterization of local ranges. Through a spatial meta-analysis of $^{87}Sr/^{86}Sr$ values from archaeological human, faunal, and artifact samples (n = 1658) from 45 publications, this study aims to quantify and compare variation in bioavailable strontium and create the first predictive isotope model (or isoscape) for $^{87}Sr/^{86}Sr$ values in the prehistoric Andes. Descriptive statistics, including the coefficient of variation, are compared between sites from different temporal categories, and between coastal, yungas, and highland sites. Regional differences in the $^{87}Sr/^{86}Sr$ values of male and female biological sex categories are compared for human enamel and bone samples, and between sequentially-forming enamel and bone samples. The study finds that the archaeological dataset trimmed of outliers provides a reliable model of local ranges. However, we caution that when migration and trade networks being investigated are within homogeneous isoscape regions, or between contiguous neighbors, multiple isotopic signatures should be incorporated into provenience estimations.

1. Introduction

Over the past two decades, analysis of radiogenic strontium isotopes ($^{87}Sr/^{86}Sr$) in archaeological samples has become a robust method for identifying non-local individuals or samples deposited within an archaeological site. This biogeochemical analysis is so effective at elucidating geographic residence and paleomobility processes that Larsen (2018: 871) credits it as one of the four major revolutions in bioarchaeology. Because the strontium isotopes that substitute for calcium in the hydroxyapatite crystals of bone and tooth enamel are virtually unchanged from the food chain, strontium isotope analysis provides a time capsule reflecting geographically-bound food consumption (Bentley, 2006; Knudson et al., 2014; Price et al., 2002; Slovak and Paytan, 2011). Assuming mostly local food and water sources were consumed and imbibed, sampled $^{87}Sr/^{86}Sr$ values reflect the bioavailable signature of the isotopic catchment where individuals lived during tissue formation (Crowley et al., 2017; Schwarcz et al., 2010; Valentine et al., 2008; Willmes et al., 2018). Human or animal skeletons with sub-adulthood tissue $^{87}Sr/^{86}Sr$ values that differ from the established range of their burial location would show those individuals moved (or were moved) to the burial location sometime between sub-adulthood tissue formation and death (Evans et al., 2019; Laffoon et al., 2018; Mbeki et al., 2017). When landscape $^{87}Sr/^{86}Sr$ ranges in a study region are known, strontium isotope analysis allows us to track long-term migrations and shifts in settlement strategies through time and space. This can help us understand mobility as a response to sweeping cultural or environmental changes (Borić and Price, 2013; Laffoon and Hoogland, 2012; Perry et al., 2017; Tung, 2008; Valentine et al., 2008), or show that populations were less migratory than anticipated during periods known for mobility (Knudson et al., 2012b; Stojanowski and Knudson, 2011).

Notwithstanding the promise of these analytical techniques, our ability to identify non-locals and their likely places of origin relies entirely on accurate characterization of local ranges, through statistical parsing of archaeological samples, and establishing local baselines by testing modern proxy materials. While robust baseline studies are

* Corresponding author. 900 Cady Mall, Tempe, AZ, 85287-2402, USA.
E-mail addresses: beth.scaffidi@asu.edu (B.K. Scaffidi), kelly.knudson@asu.edu (K.J. Knudson).

https://doi.org/10.1016/j.jas.2020.105121
Received 18 September 2019; Received in revised form 19 February 2020; Accepted 3 March 2020

necessary to fully define local $^{87}Sr/^{86}Sr$ values, an examination of population-wide variability at a regional scale can also shed light on the nature of paleomobility in past populations—particularly in regions where baseline sampling is logistically or contextually-problematic. For example, in the Andes, human settlements in deep coastal valleys often difficult to access for baseline sampling. Natural factors like volcanic activity, landscapes caused by earthquakes, floods, or human agricultural practices can cause local environmental $^{87}Sr/^{86}Sr$ values to deviate from past values or from underlying bedrock geology (e.g. Maurer et al., 2012; Thomsen and Andreasen, 2019). To characterize local ranges of variation in $^{87}Sr/^{86}Sr$ values throughout the prehistoric Andes, this study examines site-wide variation in published, spatially-contextualized archaeological $^{87}Sr/^{86}Sr$ samples. After briefly reviewing the principles of the strontium isotope system and the identification of non-locals based on $^{87}Sr/^{86}Sr$ values, the dataset and methods for non-spatial and spatial statistical meta-analysis are described. Variance between sites, time periods, tissue types, and biological sex are examined and an archaeological isoscape is proposed to identify discrete isotopic provinces within the prehistoric Andes.

1.1. The strontium isotope system: from bedrock to the body

Strontium is a naturally occurring trace element with four stable isotopes (^{84}Sr, ^{86}Sr, ^{87}Sr, and ^{88}Sr), one of which is also radiogenic (^{87}Sr). In bedrock, rubidium (^{87}Rb) decays into radiogenic ^{87}Sr, so that the ratio of heavier to lighter isotopes ($^{87}Sr/^{86}Sr$) varies according to geological age and composition of bedrock, particularly with respect to Rb/Sr values (Bentley, 2006; Faure and Mensing, 2005). Weathered bedrock is incorporated into soil, plants, animals, and water comprising the food chain. In addition to geological strontium from local bedrock weathering, atmospheric and surface sources like rainfall, rivers, sea-spray, wind dust, large-scale construction and quarrying activities, and anthropogenic sources like modern fertilizers contribute to the pool of bioavailable strontium in the food chain (Bataille and Bowen, 2012; Bataille et al., 2012; Bentley, 2006; Crowley et al., 2017; Fenner and Wright, 2014; Kamenov et al., 2009; Price et al., 2002; Willmes et al., 2018). A significant portion of bioavailable strontium is derived from rainwater and sea spray in coastal regions (Whipkey et al., 2000), while wind-transported dust (loess) contributes substantially to the pool of bioavailable strontium in arid regions (Bentley, 2006).

As organisms consume food and water, these multiple sources of strontium are mixed and incorporated into tissues. In vertebrates, strontium replaces calcium in the hydroxyapatite crystals of enamel and bone during tissue development. Due to their large atomic mass, strontium isotopes undergo very little fractionation from dietary sources to bodily tissues, thus accurately reflecting the bioavailable strontium in food and water consumed (Graustein, 1989). However, because strontium follows calcium pathways into the body, strontium values in omnivores can disproportionately reflect high-strontium foods, which are generally high-calcium foods, over proteins (Aufderheide, 1989; Burton and Hahn, 2016; Montgomery, 2010). Similarly, consumption of calcium-enriched foods like salt, are disproportionately reflected in the $^{87}Sr/^{86}Sr$ values tissues of the organisms that consume those foods (Bataille et al., 2012; Fenner and Wright, 2014; Hodell et al., 2004; Slovak et al., 2009; Wright, 2005). Bodily tissue $^{87}Sr/^{86}Sr$ values are generally consistent with the $^{87}Sr/^{86}Sr$ values averaged from the bioavailable isotopic catchment of the diet (Sillen et al., 1998)—which is in turn reflects the $^{87}Sr/^{86}Sr$ values of mixed geological (i.e. bedrock geology) and atmospheric contributions at any given spatial location.

Increasingly, researchers are documenting $^{87}Sr/^{86}Sr$ values in enamel apatite from sequentially-forming teeth and bone to understand mobility within the life course of individuals (Buikstra et al., 2004; Eriksson et al., 2018; Evans et al., 2006; Hrnčíř and Laffoon, 2019; Knudson et al., 2016). Tooth enamel is formed during sequential phases during infancy and childhood (Table 1), after which it is metabolically inert (Hillson, 1996). Because permanent first molar and first incisor

Table 1
Descriptive statistics by archaeological samples type (N = 1658).

Type	n	Mean $^{87}Sr/^{86}Sr$	Standard deviation (s)	Variance (s^2)	Coefficient of variation (CV)	Minimum $^{87}Sr/^{86}Sr$	Q1	Median	Q3	Maximum $^{87}Sr/^{86}Sr$	Range	IQR
Artifact	36	0.70789	0.00222	0.000005	0.31	0.70596	0.70670	0.70714	0.70790	0.71683	0.01087	0.00120
Fauna	232	0.70797	0.00281	0.000008	0.40	0.70393	0.70621	0.70717	0.70923	0.72388	0.01995	0.00302
Human	1390	0.70812	0.00218	0.000005	0.31	0.70384	0.70727	0.70769	0.70815	0.72136	0.01944	0.00088

enamel is formed mostly in utero and during the first two years of life (Hillson, 1986), bulk-sampled enamel from these teeth is heavily skewed by in utero and breastfeeding contributions of maternal diet. Bone, on the other hand, is constantly remodeled throughout life at rates that vary by skeletal element, metabolism, and pathology (Fahy et al., 2017). Due to the sequential nature of enamel and bone formation, sampling $^{87}Sr/^{86}Sr$ values in teeth from distinct developmental phases and bone reflecting the last years of life allows for a life-long residential history of individuals with these tissues preserved (Hrnčíř and Laffoon, 2019; Knudson et al., 2016).

Sequential sampling studies must consider sample preservation in the interpretation of $^{87}Sr/^{86}Sr$ values. Tooth enamel has been the preferred tissue of analysis; the larger apatite minerals and rigid, calcified matrix reduce post-depositional diagenesis (Bentley et al., 2004). Since bone hydroxyapatite is susceptible to strontium uptake from soil and water in the burial environment, bone samples can artificially show local soil or fertilizer values rather than the values of a non-local dietary catchment (Budd et al., 2000; Hedges, 2002; Price et al., 1992). Nonetheless, in some cases, non-local bone apatite values have corroborated non-local enamel apatite values (Knudson and Tung, 2011). This demonstrates that bone apatite is suitable for tracking life-long residence history, particularly in arid zones of the Andes with well-preserved archaeological tissues. Moreover, methods for detecting diagenetic contamination via trace element analysis (Grimstead et al., 2018; Kamenov et al., 2018) or laser ablation mass spectroscopy (e.g. Rasmussen et al., 2019) are continuously improving the detection of post-mortem bone alteration. Comparing the variance between enamel and bone between many sites in a study region can help us understand whether bone is generally a viable tissue for testing given the unique mix of strontium contributions to the diet in that region.

1.2. Identifying outliers by establishing local $^{87}Sr/^{86}Sr$ ranges

Methods for determining the local $^{87}Sr/^{86}Sr$ range have become increasingly complex and contested. Originally, researchers classified the local human signature based on the sample mean of archaeological tissues (bone or enamel) ± 2 sd, so that outlier values beyond this range would be classified as non-local. This is a conservative measure, unlikely to incorrectly classify non-locals, but probably underestimating the number of non-locals in a sample (Bentley et al., 2004). Others use the sample mean ± 1 sd as a less conservative threshold for defining the local range, possibly overestimating the identification of non-locals (Laffoon et al., 2017; Lofaro et al., 2019). Studies with large sample sizes often follow Wright (2005) in defining the local range as the normal distribution of archaeological human samples trimmed of outliers (Knudson and Tung, 2011; Kootker et al., 2019). However, means are sensitive to outliers and sample size, so basing local signatures on mean values, particularly in smaller samples, are subject to over- or under-estimating the local range. Furthermore, as Grimstead et al. (2017: 188) acknowledges, with larger samples comes the issue of determining where the dataset should be trimmed—and various statistical approaches for trimming (e.g. Price et al., 2015; Price et al., 1994; Wright, 2005) are based on the central limit theorem. Indeed, estimates of central tendency may not be appropriate measures for the complex and time-averaged phenomenon of human dietary practices.

Given the circular reasoning inherent in defining local signatures based on a statistically-arbitrary categorization of archaeological values (when archaeological populations cannot be assumed to have been stationary), researchers soon shifted to sampling archaeological fauna with limited home ranges to understand local variability. Because non-domesticated animals consume only locally available food and water that reflects a "regional average" of bioavailable strontium, some researchers argued that the local range should be established by the mean of archaeological and modern tooth enamel from small mammals like rabbits and mice, ± 2 sd (Bentley et al., 2004: 366, Evans and Tatham, 2004, Price et al., 2002: 124). Building on this idea, researchers soon began analyzing locally-raised, locally-fed modern fauna in addition to archaeological fauna with limited home ranges, and defining local $^{87}Sr/^{86}Sr$ signatures as the mean of those samples ±2 sd (Buzon et al., 2012; Conlee et al., 2009; Frei and Price, 2012; Grimstead et al., 2017; Knudson and Price, 2007; Knudson et al., 2004; Slovak et al., 2018). One novel, recent approach (Lengfelder et al., 2019) developed faunal baselines as a function of mixed-source contributions (from vegetation, soil, and atmospheric constributions of strontium) and measured archaeological faunal values. While these archaeological proxies for bioavilable strontium are useful in comparing the mixed strontium sources between organisms that mix those sources in similar ways, it can be difficult to determine that archaeological materials were local or fed local foods. Fertilizers in the food chain and other anthropogenic practices can alter modern or archaeological faunal $^{87}Sr/^{86}Sr$ values away from the local bioavailable signature (Maurer et al., 2012; Thomsen and Andreasen, 2019).

To avoid some of these issues, researchers have recently established local baselines by sampling environmental proxies (e.g. modern soil, water, and plants), and then constraining archaeological samples deterministically to regions with matching environmental baseline values (Frei and Price, 2012; Hedman et al., 2018; Hodell et al., 2004; Kootker et al., 2016). For example, since alluvial soils average bedrock strontium from surrounding areas, they can be used as proxies for bioavailable strontium in the food chain (Bentley, 2006; Knudson et al., 2014; Willmes et al., 2018). Water also averages strontium from soils draining into the watershed, but is susceptible to changes from precipitation and seasonal hydrological fluxes (Crowley et al., 2017; Frei and Frei, 2011; Frei and Frei, 2013; Shand et al., 2009). Similarly, because plants average strontium from soil and water, they can be an excellent proxy for bioavailable strontium in some regions (Bentley, 2006; Sillen et al., 1998; Valentine et al., 2008; Willmes et al., 2018).

The fit of environmental proxies to archaeological skeletons is highly contingent upon local geological and hydrological processes. For example, one study found modern plants were a closer fit for archaeological values than modern fauna (Maurer et al., 2012) while another shows a similar offset between soil and plant samples and archaeological samples (Valentine et al., 2008). In the Andes, Knudson et al.'s (2014) study cautions that soils may not be the best predictors for archaeological human $^{87}Sr/^{86}Sr$ values; however, there have been no pan-regional studies of baseline flora or fauna for comparison. Organismal differences in dietary preference, metabolism, and morphology (e.g. differing plant root depths) might lead to differential proportions in the mix of strontium sources between producers and different levels of consumers throughout the food web (See summary in Grimstead et al., 2017:186–187).

To this end, Grimstead (2017) suggests sampling the entire food chain via extensive field surveys. However, in places where paleoclimatic or hydrologic variability was high, or where agricultural or tectonic activity was intense, there may be no reason to suspect a close fit between archaeological and modern proxies. As Slovak and Paytan. (2011: 746) recognize, hypotheses about the proportion of locals to non-locals in an archaeological population and knowledge of local geological history must guide the strategy to define the local $^{87}Sr/^{86}Sr$ range and select outliers—in many cases, "statistical analyses of the human data is probably more effective at differentiating between local and non-local individuals."

1.3. Geolocation with strontium isoscape models

In addition to pinpointing statistical outliers among populations of samples, strontium isotopes have been successfully used to match samples with likely regions of origin based on geostatistical models. Spatially explicit predictive isotope models (isoscapes) can be based on archaeological or modern baseline materials, allowing us to interpolate isotopic ranges in places without measured values from samples at known coordinates (Bowen, 2010; Hedman et al., 2018; Kootker et al.,

2016; Pellegrini et al., 2016; Schwarcz et al., 2010). While many archaeological studies have generated deterministic models of geographically or geomorphologically-bounded ranges using baseline sample values (Fenner and Frost, 2009; Hedman et al., 2018; Kootker et al., 2016; Maurer et al., 2012), very few have applied geostatistical models—true isoscapes—to geo-locating or assigning samples to their most probable geographic origins. Notable exceptions include strontium isoscapes in South Africa (Copeland et al., 2016), the circum-Caribbean (Bataille et al., 2012; Laffoon et al., 2017), France (Willmes et al., 2018), Western Europe (Bataille et al., 2018; Grupe et al., 2017), central Turkey (Meiggs et al., 2017), and Australia (Adams et al., 2019). However, most of these studies rely entirely on environmental proxies to predict measured skeletal values (except for Grupe et al., 2017). The mixing of multiple strontium end-member contributions in an organism may be best modeled by the target organisms themselves: archaeological plants, humans, and fauna. Thus, isoscapes generated from measurements of archaeological samples can provide accurate predictions for sample geolocation (Lengfelder et al., 2019).

As Pellegrini et al. (2016) demonstrated for the spatial distribution of oxygen isotopes in archaeological human enamel across prehistoric Britain, modeling the distribution and variability in archaeological isotope values is useful in and of itself. Comparing archaeological values to each other directly through a predictive isotope or isoscape model enables a geographic determination of bioavailable $^{87}Sr/^{86}Sr$ variability independent of landscape factors that could complicate local signatures. Here, the range and variance of $^{87}Sr/^{86}Sr$ values from provenienced archaeological samples is used to compare site-wide heterogeneity between sites throughout the prehistoric Andes. Because human and animal skeletons, and archaeological plants, reflect the mixed sources of bioavailable strontium they consume, they can be used to define the potential range of bioavailable $^{87}Sr/^{86}Sr$ values throughout a broad geographic region where environmental baselines are difficult to procure and model. Furthermore, comparing population-level and intra-lifetime $^{87}Sr/^{86}Sr$ variability across a region can show how cultural practices and the environment might have structured mobility characteristics of individuals of different biological sex, occupation, or ethnic groups. To that end, this study compiles and compares $^{87}Sr/^{86}Sr$ signatures from published archaeological data to clarify broad population-wide spatiotemporal patterns of $^{87}Sr/^{86}Sr$ variability in the prehistoric Andes.

1.4. Baseline $^{87}Sr/^{86}Sr$ models in the andes

While $^{87}Sr/^{86}Sr$ values from exposed bedrock and water have been extrapolated into reference maps for the Andes (See summary in Knudson et al., 2014: 207–208), there are a number of obstacles to applying these models to constrain archaeological sample residential origins. First, bedrock $^{87}Sr/^{86}Sr$ values have not been directly sampled in many regions. This leads to bedrock-only models showing large swaths of homogeneous expected $^{87}Sr/^{86}Sr$ values, due either to small sample size or true geological homogeneity (Schenk et al., 1999) (Fig. 1.). Second, the error rates of bedrock model predictions for the actual isotopic catchments of geologically-diverse regions are high. Unrelenting volcanism and tectonic activity over the last 20 million years resulted in complex formation processes. The contamination of igneous rocks by varying kinds of crustal material or oceanic sediments (Klerkx et al., 1977) contribute to heavy isotope signatures that differ sharply even within seemingly geologically-similar regions (Kamenov et al., 2002; Macfarlane et al., 1990; Mamani et al., 2008). Third, heavy reliance on seafood in the diet can also cause skeletal $^{87}Sr/^{86}Sr$ values to deviate from the local baseline, when strontium from marine sources is frequently consumed by humans or the animals consumed by humans (Slovak et al., 2009; Wright, 2005).

In addition to the complexities of modeling the bedrock contributions to the overall strontium catchment, Andean soils collect a significant amount of aeolian dust from distant places. In fact, the Bolivian altiplano and Patagonia comprise two of the ten most prolific dust-producing places globally (Taylor, 2002). Anthropogenic burning is known to be a cause of wind-transported dust deposits in the modern Andes (Estevan et al., 2019). These factors might contribute to the mismatch between modern soil, plants, and fauna and bedrock $^{87}Sr/^{86}Sr$ values in the Andes reported by Knudson and Torres-Rouff (2014). Process-based strontium isoscapes based on modern baseline samples are in development by the authors and other researchers. These will continue to shape our understanding of bedrock, soil, and mixed-sources of strontium in isotopic catchments. In the meantime, analyzing site-wide and intra-individual variability in archaeological $^{87}Sr/^{86}Sr$ values is a critical first step to understanding the influences of dietary and mobility practices on averaged end-member tissue $^{87}Sr/^{86}Sr$ values.

2. Materials and methods

This study is a spatial meta-analysis of $^{87}Sr/^{86}Sr$ values from archaeological human, faunal, and artifacts (fauna, wood, and other botanicals) from modern-day Argentina, Bolivia, Chile, and Peru published before August 2019.[1] After duplicates from overlapping datasets were eliminated, the dataset includes 1658 samples from 45 publications (Andrushko et al., 2009; Barberena et al., 2017; Bethard et al., 2008; Buzon et al., 2012; Chala-Aldana et al., 2018; Conlee et al., 2009; Durán et al., 2018; Hewitt, 2013; Juengst, 2017; Juengst et al., 2015; Knudson, 2008; Knudson and Buikstra, 2007; Knudson et al., 2012a; Knudson et al., 2017; Knudson et al., 2012c; Knudson and Price, 2007; Knudson et al., 2004; Knudson et al., 2016; Knudson and Torres-Rouff, 2014; Knudson and Torres-Rouff, 2015; Knudson and Torres-Rouff, 2009; Knudson and Tung, 2011; Knudson and Tung, 2007; Knudson et al., 2005; Knudson et al., 2014; Knudson et al., 2009; Kurin et al., 2016; Lofaro et al., 2019; Lucas, 2012; Mader et al., 2018; Marsteller et al., 2017; Nado et al., 2012; Slovak et al., 2018; Slovak et al., 2009; Standen et al., 2018; Stanish et al., 2018; Takigami et al., 2019; Thornton et al., 2011; Tomczyk et al., 2019; Torres-Rouff and Knudson, 2007; Torres-Rouff and Knudson, 2017; Torres-Rouff et al., 2015; Tung and Knudson, 2008; Turner et al., 2009; Webb, 2010; Wylde, 2017) (Table S1). The accuracy and precision of these data and the international standards employed are reported in the original publications; based on the accuracy and precision of the data generated using international and readily available standards, as well as the availability of assessments for diagenetic contamination employed in these studies, these data can be reliably compared and combined.

2.1. Database coding

The database recorded sample type (artifact, fauna, or human), site names, time periods, estimated biological sex and age-at-death, tissue type (tooth or bone), and the developmental sequence of sampled tissue (defined immediately below). Probable males or females were collapsed into the male and female categories for statistical testing. Year ranges of sites were collapsed following Rowe and Menzel's (1967) absolute chronology, as follows: Archaic (2000 BCE and older), Early Horizon (*ca.* 500–2000 BCE), Early Intermediate Period or EIP (*ca.* 200 BCE – 600 CE), Middle Horizon (*ca.* 600–1100 CE), Late Intermediate Period or LIP (*ca.* 1100–1400 CE), Late Horizon (1400–1532 CE), or not reported (NR).[2]

[1] There were no archaeological data points from Ecuador or Columbia.

[2] Rowe's chronological categories have been appropriately critiqued as not pertinent to localized cultural changes in specific regions of the Andes, and are particularly problematic outside of Peru (See contributions in Swenson and Roddick, 2018). Nonetheless, they are widely understood across the Andes, are the most commonly used in the studies we investigated, and they provide a convenient heuristic sequence for comparing changes through time in site-wide variance of radiogenic isotopic signatures.

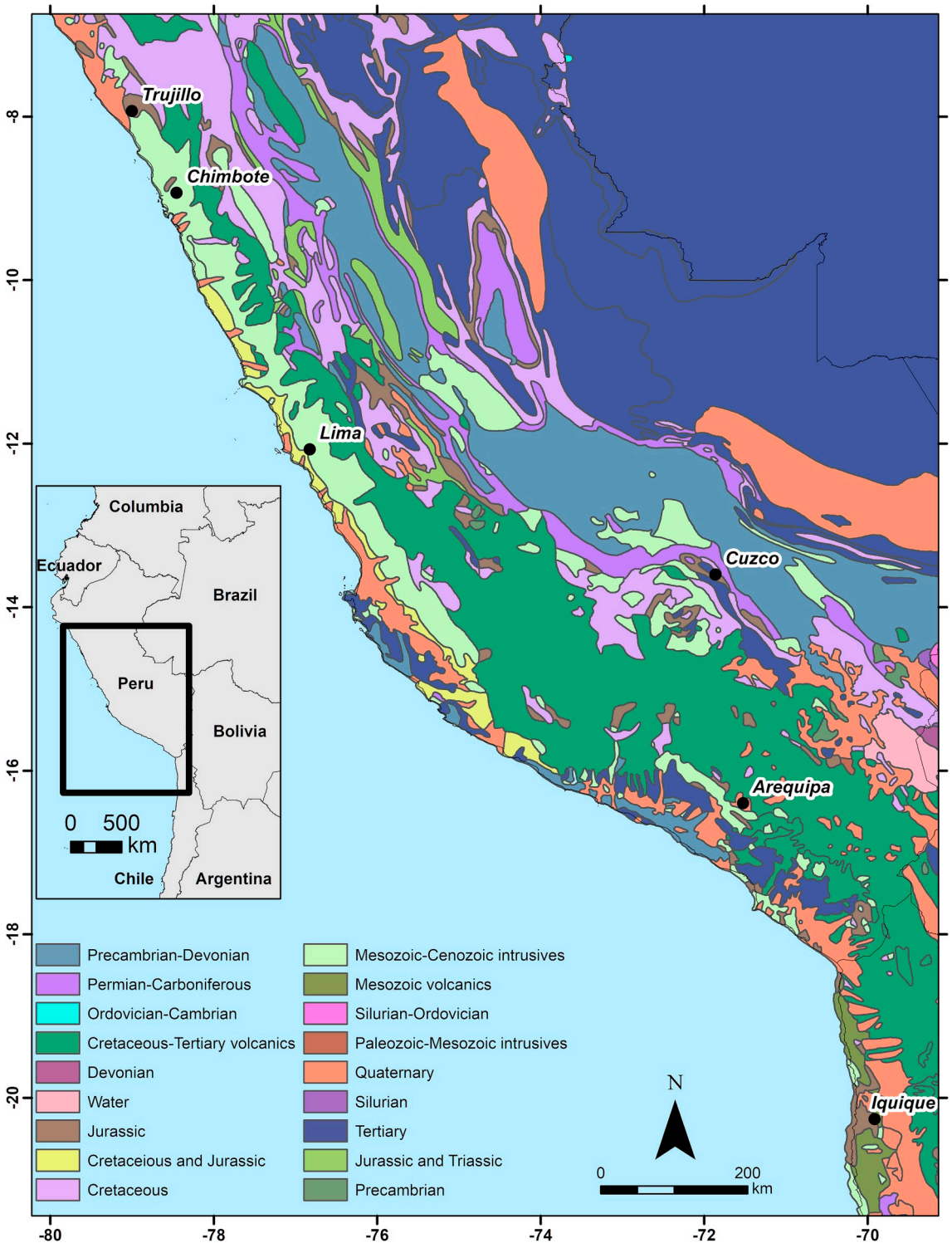

Fig. 1. Bedrock geology map (Schenk et al., 1999). Grid shows latitude and longitude.

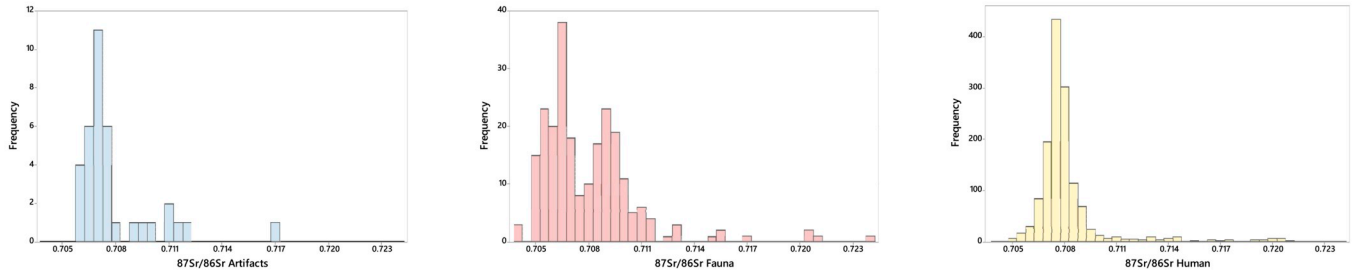

Fig. 2. Histograms of $^{87}Sr/^{86}Sr$ values for the artifact, faunal, and human subsamples.

To enable comparisons between childhood and adulthood residential mobility across the entire dataset, teeth were designated according to the typical developmental period of crown enamel (Hillson, 1986, 1996). Adult teeth were categorized as: infancy/early childhood (incisors and first molars), middle childhood (canines, premolars, and second molars) and teen (third molars). Deciduous teeth and one dentin sample were excluded from statistical tests. For individuals with multiple teeth from the same developmental phase, or multiple samples from the same tissue, each individual $^{87}Sr/^{86}Sr$ value was considered a distinct measurement—e.g. samples were not averaged per individual, sample type, or life course phase. If a molar could not be identified as first, second, or third, it was used as a data point in the isoscape model but excluded from statistical testing. All bone samples were coded as late life, but bone-enamel comparisons were limited to adult bone, since subadult bone theoretically duplicates some portion of the enamel signature from late-forming teeth, depending on the age-at-death.

2.2. Statistical analysis

Descriptive statistics were compiled in Minitab 19 (Minitab, LLC). $^{87}Sr/^{86}Sr$ values were rounded to four decimal places before statistical analysis, as differences beyond the fifth decimal place are likely due to intra-individual variation or instrumental uncertainty between and within laboratories (Knudson et al., 2016: 595). Heterogeneity was compared between sites by calculating the site-wide standard deviation (s), variance (s^2), as well as the sample-size corrected coefficient of variation (CV), since that measure enables the direct comparison of multiple samples while minimizing the distorting effects of outliers. The coefficient of variation was computed as $CV = (1 + 1/4n)\ (100s/\ \bar{x})$, where n = sample size, s = sample standard deviation, and $\bar{x}$ = sample mean. A rough proxy of population diversity was generated by computing the percentage of each site's total number of samples that fell outside the mean ± 2 SD (the most conservative measure of outliers).

Statistical tests were completed in Minitab 19. Distribution of data was assessed with the Ryan-Joiner test for normality. The spread and variance of these normally distributed datasets were compared by computing the ratio of site variance with the F-test (ANOVA) for two samples. Bartlett's test for homogeneity of variances was used to compare variance between more than two samples. When a significant difference was detected, confidence intervals were compared with pairwise Bonferroni testing to determine which sample variances were distinct. Chi-squared was used to compare relative proportions of statistical outliers between sites. The significance level (α) was 0.05 for all tests.

2.3. Spatial and geostatistical analysis

To understand spatial variation in $^{87}Sr/^{86}Sr$ values, site coordinates were first plotted in ArcMap 6.1 and projected to the Albers South America Equal Area Conic coordinate system, which minimizes distortion over the exceptional latitudinal range in the study. Sites within 1 km of each other were collapsed and data points without site coordinates verifiable to within a 1 km range of accuracy after reviewing pertinent literature were excluded from geostatistical analysis. To compare the potential environmental and cultural effects of altitudinal location on variance in strontium signatures, site elevations in meters above sea level (masl) were extracted from the ASTER Digital Elevation Model (version 2) (Tachikawa et al., 2011), and each site was classified as coastal (0–500), yunga (500–2300), or highland (over 2300 masl),[3] according to the biogeographical zones of Pulgar Vidal (1981) (Table S1). All subsequent geostatistical analysis was carried out with ArcMap 6.1.

Because the mixed-source $^{87}Sr/^{86}Sr$ signatures in tissues and plants are assumed to be continuously variable across landscapes, geostatistical methods were used to establish outlier $^{87}Sr/^{86}Sr$ values (Following Pellegrini et al., 2016). Moran's I, a global measure of spatial autocorrelation, was calculated in order to satisfy the threshold requirements of geostatistical modeling (Cressie, 1993; Oliver and Webster, 1990, 2014, 2015). Cluster/outlier analysis was completed with Anselin's Local Moran's I, following Pellegrini et al.'s methodology and rationale (2016: 4). High values surrounded by unusually low values and low values surrounded by unusually high values were defined as spatial outliers and excluded from the subsequent isoscape model.

The archaeological predictive isoscape model was generated using Universal Kriging, a geostatistical interpolation method that estimates values for non-sampled locations by weighting averages of closer samples more heavily than distant samples (Cressie, 1993). All coincidental $^{87}Sr/^{86}Sr$ points were modeled rather than averaging site-wide samples prior to modeling. Universal Kriging was used since the $^{87}Sr/^{86}Sr$ values showed an east-west trend—the trend was modeled using a first-order local polynomial interpolation and removed from the data (Oliver and Webster, 1990, 2014, 2015). The semivariogram (a dissimilarity function describing the distance at which samples cease spatial autocorrelation) (Cressie, 1993) was modeled on the residuals with the parameters indicated in Table S2 and added back after interpolation (Johnston et al., 2001). The model fit to the data was assessed with leave-one-out cross-validation within the Geostatistical Wizard tool in ArcMap, which estimated the trend and autocorrelation of the data (Johnston et al., 2001). The fit of the predicted to measured values of the model was assessed using the parameters in Table S2. Validation was performed by removing 10% of the dataset, trimmed of spatial outliers (n = 155), as a test set and running the model again with the same parameters on the training dataset (n = 1391). Model parameters are reported in Table S2 following Fisher and colleagues (Fisher et al., 2010).

[3] Pulgar Vidal's highest elevational zones (*quechua* [2300–3500 masl], *suni* [3500–4100 masl], and *janca* [over 4100 masl] were collapsed into one highland category.

Table 2
Comparison of different measures of site-wide heterogeneity in $^{87}Sr/^{86}Sr$ across all archaeological samples (n = 81 sites).

Site	Total (n)	Mean $^{87}Sr/^{86}Sr$	Standard deviation (s)	Variance (s^2)	Coefficient of variation (CV)	Minimum $^{87}Sr/^{86}Sr$	Q1	Q3	Maximum $^{87}Sr/^{86}Sr$	Range	IQR	2 SD Range	# samples outside of 2 SD	% of samples outside of 2 SD
Acha 3	2	0.7087	0.0001	0.0000	0.01	0.7086	*	*	0.7087	0.0001	*	0.7085–0.7088	*	*
Aja	1	0.7067	*	*	*	0.7067	*	*	0.7067	*	*	*	*	*
Ancon	64	0.7078	0.0005	0.0000	0.06	0.7056	0.7077	0.7080	0.7084	0.0029	0.0003	0.7069–0.7087	3	4.7
Armatambo	118	0.7075	0.0003	0.0000	0.04	0.7069	0.7074	0.7077	0.7083	0.0014	0.0003	0.7070–0.7081	8	6.8
B.61	5	0.7069	0.0004	0.0000	0.06	0.7066	0.7066	0.7073	0.7075	0.0009	0.0006	0.7061–0.7077	0	0.0
Barrio Ramos	4	0.7091	0.0004	0.0000	0.05	0.7087	0.7087	0.7095	0.7095	0.0009	0.0007	0.7084–0.7098	0	0.0
Beringa	58	0.7084	0.0003	0.0000	0.04	0.7078	0.7083	0.7084	0.7096	0.0018	0.0001	0.7079–0.7089	3	5.2
Cachi	14	0.7071	0.0005	0.0000	0.07	0.7057	0.7070	0.7074	0.7078	0.0021	0.0004	0.7062–0.7081	1	7.1
Cahuachi	56	0.7065	0.0005	0.0000	0.08	0.7059	0.7062	0.7067	0.7087	0.0027	0.0005	0.7054–0.7076	2	3.6
Camarones	5	0.7087	0.0001	0.0000	0.01	0.7086	0.7087	0.7088	0.7089	0.0002	0.0002	0.7086–0.7089	0	0.0
Cantayo	6	0.7071	0.0010	0.0000	0.14	0.7063	0.7063	0.7081	0.7089	0.0026	0.0018	0.7051–0.7092	0	0.0
Capiz Alto	6	0.7075	0.0004	0.0000	0.06	0.7071	0.7072	0.7080	0.7081	0.0010	0.0008	0.7067–0.7083	0	0.0
Casa Paroquial	36	0.7084	0.0018	0.0000	0.25	0.7075	0.7077	0.7079	0.7146	0.0070	0.0002	0.7049–0.7118	3	8.3
Caspana	30	0.7077	0.0004	0.0000	0.05	0.7071	0.7076	0.7077	0.7096	0.0026	0.0001	0.7069–0.7085	1	3.3
Castillo de Huarmey	87	0.7073	0.0014	0.0000	0.20	0.7049	0.7071	0.7075	0.7172	0.0123	0.0005	0.7045–0.7100	2	2.3
Cayo Oriental	1	0.7077	*	*	*	0.7077	*	*	0.7077	*	*	*	*	*
Cerro Baul	11	0.7070	0.0016	0.0000	0.22	0.7059	0.7061	0.7068	0.7116	0.0058	0.0007	0.7038–0.7101	1	9.1
Cerro del Gentil	81	0.7072	0.0012	0.0000	0.17	0.7060	0.7069	0.7073	0.7168	0.0109	0.0003	0.7047–0.7096	1	1.2
Cerro Tunduqueral	1	0.7086	*	*	*	0.7086	*	*	0.7086	*	*	*	*	*
Chavin	11	0.7104	0.0017	0.0000	0.24	0.7064	0.7098	0.7113	0.7122	0.0058	0.0015	0.7080–0.7094	1	9.1
Chen Chen	66	0.7078	0.0025	0.0000	0.35	0.7019	0.7068	0.7074	0.7192	0.0173	0.0005	0.7053–0.7103	4	6.1
Chinchorro 1	2	0.7089	0.0000	0.0000	0.00	0.7089	*	*	0.7089	0.0000	*	0.7033–0.7118	*	*
Chiribaya Alta	36	0.7080	0.0017	0.0000	0.24	0.7069	0.7074	0.7080	0.7171	0.0102	0.0006	0.7089–0.7089	1	2.8
Chiribaya Baja	10	0.7073	0.0006	0.0000	0.08	0.7066	0.7067	0.7079	0.7080	0.0015	0.0013	0.7047–0.7114	0	0.0
Ch'isi	23	0.7087	0.0004	0.0000	0.05	0.7082	0.7085	0.7089	0.7097	0.0015	0.0004	0.7061–0.7085	2	8.7
Chokepukio	63	0.7102	0.0037	0.0000	0.52	0.7073	0.7081	0.7105	0.7214	0.0141	0.0024	0.7029–0.7175	5	7.9
Collanco	4	0.7064	0.0005	0.0000	0.06	0.7058	0.7059	0.7068	0.7068	0.0010	0.0008	0.7055–0.7073	0	0.0
Colon 10	1	0.7087	*	*	*	0.7087	*	*	0.7087	*	*	*	*	*
Conchopata	19	0.7065	0.0012	0.0000	0.17	0.7055	0.7057	0.7067	0.7102	0.0047	0.0011	0.7040–0.7089	1	5.3
Coyo 3	14	0.7077	0.0003	0.0000	0.04	0.7068	0.7077	0.7078	0.7080	0.0011	0.0002	0.7072–0.7082	1	7.1
Coyo Oriental	26	0.7077	0.0003	0.0000	0.04	0.7070	0.7076	0.7079	0.7082	0.0012	0.0002	0.7072–0.7082	2	7.7
Cuncaicha	13	0.7063	0.0001	0.0000	0.02	0.7062	0.7063	0.7064	0.7066	0.0004	0.0002	0.7061–0.7066	1	7.7
Cundisa	8	0.7080	0.0005	0.0000	0.07	0.7071	0.7078	0.7083	0.7086	0.0015	0.0005	0.7071–0.7090	0	0.0
Cutamalla	22	0.7056	0.0009	0.0000	0.12	0.7050	0.7052	0.7055	0.7090	0.0040	0.0003	0.7039–0.7073	1	4.5
Hakenasa	2	0.7068	0.0000	0.0000	0.00	0.7068	*	*	0.7069	0.0000	*	0.7068–0.7069	*	*
Iwawe	3	0.7097	0.0010	0.0000	0.14	0.7089	0.7089	0.7108	0.7108	0.0019	0.0019	0.7077–0.7117	0	0.0
Jauranga	8	0.7064	0.0010	0.0000	0.15	0.7052	0.7055	0.7068	0.7085	0.0033	0.0013	0.7043–0.7085	0	0.0
Juch'uypampa	3	0.7130	0.0009	0.0000	0.12	0.7124	0.7124	0.7140	0.7140	0.0016	0.0016	0.7112–0.7148	0	0.0
Kanamarca	2	0.7066	0.0001	0.0000	0.01	0.7065	*	*	0.7067	0.0001	*	0.7064–0.7068	*	*
Khonkho Wankane	5	0.7089	0.0002	0.0000	0.03	0.7087	0.7087	0.7091	0.7092	0.0005	0.0003	0.7085–0.7093	0	0.0
Kirawi	4	0.7102	0.0021	0.0000	0.30	0.7078	0.7082	0.7123	0.7128	0.0050	0.0041	0.7060–0.7144	0	0.0
La Tiza	40	0.7065	0.0003	0.0000	0.05	0.7056	0.7063	0.7067	0.7075	0.0019	0.0003	0.7058–0.7072	3	7.5
Laguna del Diamante	4	0.7054	0.0003	0.0000	0.04	0.7050	0.7051	0.7056	0.7056	0.0006	0.0005	0.7048–0.7059	0	0.0
Larache	37	0.7099	0.0034	0.0000	0.48	0.7076	0.7077	0.7138	0.7205	0.0128	0.0061	0.7032–0.7167	1	2.7
Las Cuevas	1	0.7067	*	*	*	0.7067	*	*	0.7067	*	*	*	*	*
Lauca	1	0.7069	*	*	*	0.7069	*	*	0.7069	*	*	*	*	*
Los Azules	1	0.7039	*	*	*	0.7039	*	*	0.7039	*	*	*	*	*
Los Queltehues	1	0.7040	*	*	*	0.7040	*	*	0.7040	*	*	*	*	*
Machu Picchu	51	0.7107	0.0049	0.0000	0.68	0.7038	0.7073	0.7134	0.7212	0.0173	0.0061	0.7010–0.7204	3	5.9

(*continued on next page*)

Table 2 (*continued*)

Site	Total (n)	Mean $^{87}Sr/^{86}Sr$	Standard deviation (s)	Variance (s^2)	Coefficient of variation (CV)	Minimum $^{87}Sr/^{86}Sr$	Q1	Q3	Maximum $^{87}Sr/^{86}Sr$	Range	IQR	2 SD Range	# samples outside of 2 SD	% of samples outside of 2 SD
Maestranza CH	4	0.7090	0.0001	0.0000	0.02	0.7089	0.7089	0.7091	0.7092	0.0003	0.0002	0.7087–0.7092	0	0.0
Majoro Chico	5	0.7067	0.0004	0.0000	0.06	0.7063	0.7063	0.7072	0.7073	0.0010	0.0008	0.7058–0.7076	0	0.0
Manzano	1	0.7040	*	*	*	0.7040	*	*	0.7040	*	*	*	*	*
Moro	15	0.7088	0.0001	0.0000	0.02	0.7085	0.7087	0.7089	0.7089	0.0004	0.0002	0.7086–0.7090	1	6.7
Pacopampa	51	0.7081	0.0020	0.0000	0.29	0.7051	0.7063	0.7096	0.7131	0.0080	0.0032	0.7040–0.7122	2	3.9
Pajonal Alto	4	0.7069	0.0008	0.0000	0.11	0.7059	0.7061	0.7076	0.7077	0.0018	0.0015	0.7054–0.7085	0	0.0
Paredones	1	0.7064	*	*	*	0.7064	*	*	0.7064	*	*	*	*	*
Patapatane	4	0.7073	0.0007	0.0000	0.10	0.7068	0.7068	0.7080	0.7083	0.0015	0.0012	0.7058–0.7087	0	0.0
Piñami	16	0.7186	0.0040	0.0000	0.55	0.7094	0.7185	0.7205	0.7239	0.0145	0.0020	0.7107–0.7265	2	12.5
Playa Miller 8	7	0.7090	0.0001	0.0000	0.01	0.7088	0.7090	0.7091	0.7091	0.0003	0.0001	0.7088–0.7092	0	0.0
Pucullu	10	0.7081	0.0012	0.0000	0.18	0.7071	0.7075	0.7083	0.7107	0.0036	0.0008	0.7056–0.7105	1	10.0
Qhota Pata	1	0.7067	*	*	*	0.7067	*	*	0.7067	*	*	*	*	*
Qopakati	4	0.7075	0.0001	0.0000	0.02	0.7073	0.7074	0.7076	0.7076	0.0003	0.0003	0.7072–0.7078	0	0.0
Quiani 7	1	0.7089	*	*	*	0.7089	*	*	0.7089	*	*	*	*	*
Quitor 5	29	0.7079	0.0005	0.0000	0.07	0.7073	0.7077	0.7079	0.7098	0.0025	0.0002	0.7069–0.7089	2	6.9
Quitor 6	2	0.7077	0.0001	0.0000	0.01	0.7077	*	*	0.7078	0.0001	*	0.7076–0.7079	*	*
Ranracancha	10	0.7079	0.0005	0.0000	0.07	0.7074	0.7076	0.7081	0.7092	0.0018	0.0005	0.7069–0.7090	1	10.0
Rinconada Alta	60	0.7075	0.0008	0.0000	0.11	0.7067	0.7072	0.7075	0.7131	0.0065	0.0003	0.7059–0.7090	1	1.7
Rio Muerto	58	0.7080	0.0020	0.0000	0.29	0.7066	0.7071	0.7079	0.7202	0.0136	0.0008	0.7040–0.7121	3	5.2
San Geronimo	4	0.7073	0.0002	0.0000	0.02	0.7070	0.7071	0.7074	0.7074	0.0004	0.0003	0.7069–0.7076	0	0.0
Santa Rita B	4	0.7051	0.0001	0.0000	0.01	0.7050	0.7050	0.7052	0.7052	0.0002	0.0002	0.7049–0.7053	0	0.0
Solcor 3	50	0.7082	0.0007	0.0000	0.10	0.7076	0.7078	0.7082	0.7125	0.0049	0.0003	0.7067–0.7096	1	2.0
Solcor Plaza	16	0.7084	0.0012	0.0000	0.17	0.7077	0.7077	0.7082	0.7110	0.0033	0.0004	0.7059–0.7108	2	12.5
Solor 3	20	0.7086	0.0021	0.0000	0.29	0.7078	0.7080	0.7083	0.7173	0.0095	0.0002	0.7045–0.7127	1	5.0
Tawa Qenani	2	0.7088	0.0000	0.0000	0.00	0.7088	*	*	0.7088	0.0000	*	0.7088–0.7088	*	*
Tchecar	59	0.7080	0.0007	0.0000	0.10	0.7076	0.7077	0.7079	0.7122	0.0046	0.0002	0.7065–0.7094	3	5.1
Tilata	2	0.7090	0.0010	0.0000	0.15	0.7082	*	*	0.7097	0.0015	*	0.7069–0.7110	*	*
Tilviche	9	0.7077	0.0007	0.0000	0.10	0.7065	0.7073	0.7079	0.7092	0.0026	0.0005	0.7063–0.7090	1	11.1
Tiwanaku	61	0.7101	0.0018	0.0000	0.26	0.7070	0.7092	0.7107	0.7163	0.0093	0.0015	0.7064–0.7137	4	6.6
Tucume	59	0.7079	0.0006	0.0000	0.08	0.7050	0.7077	0.7081	0.7094	0.0044	0.0004	0.7067–0.7090	2	3.4
Turpo	9	0.7073	0.0001	0.0000	0.02	0.7071	0.7071	0.7073	0.7074	0.0004	0.0002	0.7070–0.7075	0	0.0
Yaral	13	0.7079	0.0028	0.0000	0.40	0.7068	0.7069	0.7075	0.7174	0.0105	0.0005	0.7023–0.7136	1	7.7

* Indicates cell could not be calculated due to small sample size.

3. Results

Across the prehistoric Andes, archaeological $^{87}Sr/^{86}Sr$ values show a limited range from $^{87}Sr/^{86}Sr = 0.70384$ to $^{87}Sr/^{86}Sr = 0.72388$ ($\sigma = 0.00228$, $\sigma^2 = 0000005$, CV = 0.32, N = 1658). Descriptive statistics are reported by sample type in Table 1. The Normal QQ plot for the measured archaeological dataset shows the greatest departure from the normal distribution at Chokepukio, Machu Picchu, and Piñami in the highlands, and the greatest under-estimation at sites between Santiago, Chile and Mendoza, Argentina.

Examining $^{87}Sr/^{86}Sr$ measurements by type, the artifact $^{87}Sr/^{86}Sr$ values are normally distributed (Ryan-Joiner = 0.834, p-value < 0.010, n = 36), and the modal bin of values is $^{87}Sr/^{86}Sr = 0.7068–0.7073$ (Fig. 2a). Faunal $^{87}Sr/^{86}Sr$ values are normally distributed (Ryan-Joiner = 0.895, p-value < 0.010, n = 232) and the modal bin of values is from $^{87}Sr/^{86}Sr = 0.7063–0.70680$ (Fig. 2b). Human $^{87}Sr/^{86}Sr$ values are also normally distributed (Ryan-Joiner = 0.762, p-value < 0.010, n = 1390), and the modal bin is $^{87}Sr/^{86}Sr = 0.70725–0.70775$, followed by $^{87}Sr/^{86}Sr = 0.70725–0.70825$ (Fig. 2c). The variance of the faunal subsample (Table 1) was significantly higher than the human and artifact subsamples (Bartlett's test statistic = 29.15, p < 0.001). Small, non-migratory fauna were less variable in $^{87}Sr/^{86}Sr$ values (s = 0.004, n = 45) than large, migratory animals like camelids and dogs (s = 0.002, n = 187) (F-test, p < 0.0001). However, the variation of the migratory animal sample was not distinct from the human sample (F-test, p = 0.369), which suggests migratory animals are no worse of a proxy for local $^{87}Sr/^{86}Sr$ values than humans in the broad study region.

3.1. Comparing intra-site variance between sites

There were 79 sites with 10 or more samples—the number of samples necessary for calculating and comparing site-wide variance (Table 2, Fig. 3). Site-wide standard deviations (s) ranged from 0.0000 to 0.0824, with corresponding coefficients of variation (CV) from 0.01 to 0.68. The five archaeological sites with the greatest variation (CV) were (not in order of variation—see Table 2): Machu Picchu and Chokepukio in Cusco, Yaral in the Late Intermediate Period Ilo Valley, Piñami in Middle Horizon Lake Titicaca, and Larache in Middle Horizon San Pedro de Atacama, Chile.

Using the proportion of outliers defined conservatively as beyond the site mean ± 2 SD yielded five distinct sites with the highest proportions of inter-site outliers. Using this interval method of defining outliers, there were only 79 outliers across the entire dataset (Table 2). Comparing the relative proportions of outliers across sites showed that Piñami and Solcor Plaza (Middle Horizon San Pedro de Atacama) had the highest relative proportions of 2 SD outliers (12.5%), followed by Tilviche in the Archaic Northern Chilean desert (11.1%), and Pucullu and Ranracancha in the Late Intermediate Period Apurimac Valley (10%). It is notable that sites with the top five highest proportions of outliers as calculated with the 2 SD method are from relatively small sample sizes of 16 individuals or less.

Box plots for the 79 sites that could be mapped show relatively constrained ranges by site, with varying proportions of outliers beyond the inter-quartile range (IQR). Sites with the broadest IQR included the Early Horizon capital of Chavin, the EIP highland site of Pacopampa, the Middle Horizon San Pedro de Atacama site of Larache, and the Late Horizon Inca heartland sites of Chokepukio and Machu Picchu. Notwithstanding these broad ranges, the following sites show few to no outliers: Chokepukio shows 6 outliers, Chavin shows 1, and Larache and Pacopampa show none.

Of the 1640 samples from 64 sites with reliable coordinates, most were recovered from highland sites (681/1640 = 41.5%), as compared to coast (582/1640 = 35.5%) and *yunga* zones (377/1640 = 23.0%) (Fig. 4). Coastal sites showed a smaller standard deviation (s = 0.0006) than yunga (s = 0.001) and highland sites (s = 0.001) (Bartlett's test statistic = 479.27, p < 0.001).

3.2. Temporal variation in $^{87}Sr/^{86}Sr$ heterogeneity

Site-wide variance in $^{87}Sr/^{86}Sr$ values is distinct between time periods (Fig. 5). Sites dating to before the EIP (n = 90 samples from 4 sites) and to the EIP (n = 199 samples from 6 sites) and LIP (n = 311 samples from 11 sites) show narrow inter-quartile ranges with low numbers of outliers compared to the Middle Horizon (n = 695 samples from 20 sites) and Late Horizon (n = 196 samples from 4 sites). Table 3 compares the relative proportion of IQR outliers within sites from each temporal category (also reflected in Fig. 5).

Sites dating to the EIP and Middle Horizon have greater relative proportions of IQR outliers than sites from the other time periods. Only 1.1% (1/90) of pre-EIP samples were classified as IQR outliers, as compared to 5.5% (17/311) of LIP samples, 10.7% (21/196) of Late Horizon samples, 11.7% (81/695) of Middle Horizon samples, and 13.6% (27/199) of EIP samples (Chi-squared = 20.2655, p = 0.0004, n = 1491).

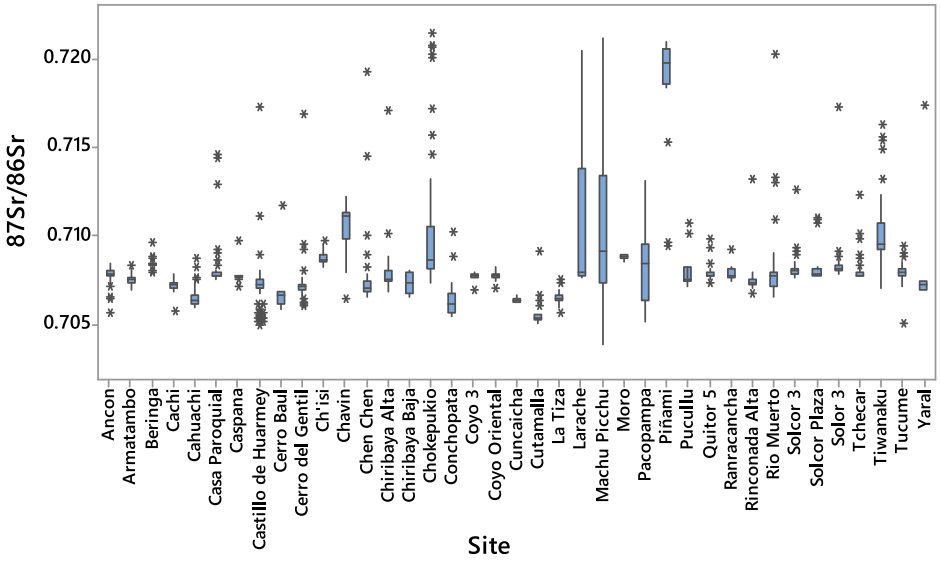

Fig. 3. Boxplot of $^{87}Sr/^{86}Srr$ values for sites with more than 10 measurements.

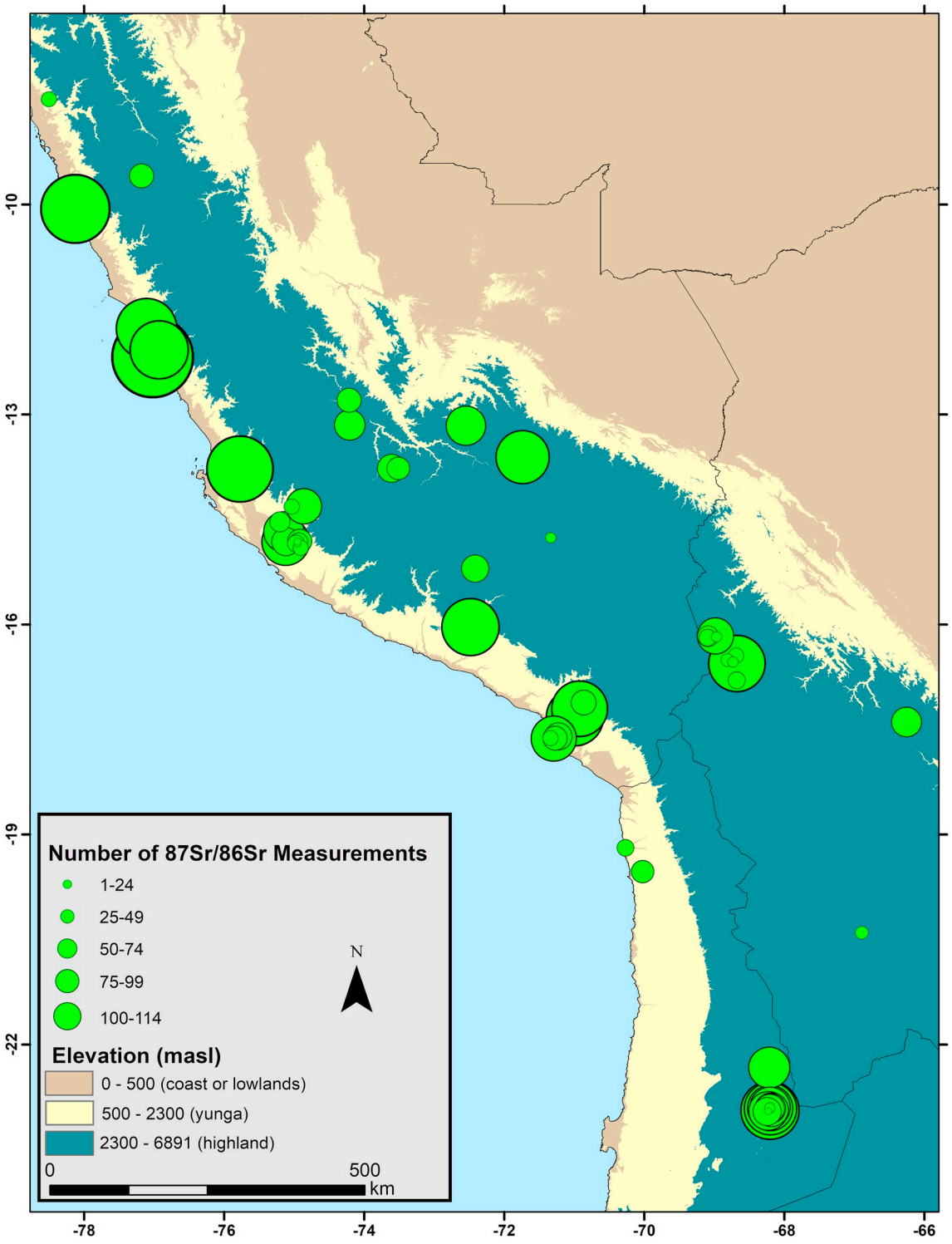

Fig. 4. Locations of $^{87}Sr/^{86}Sr$ measurements from published literature.

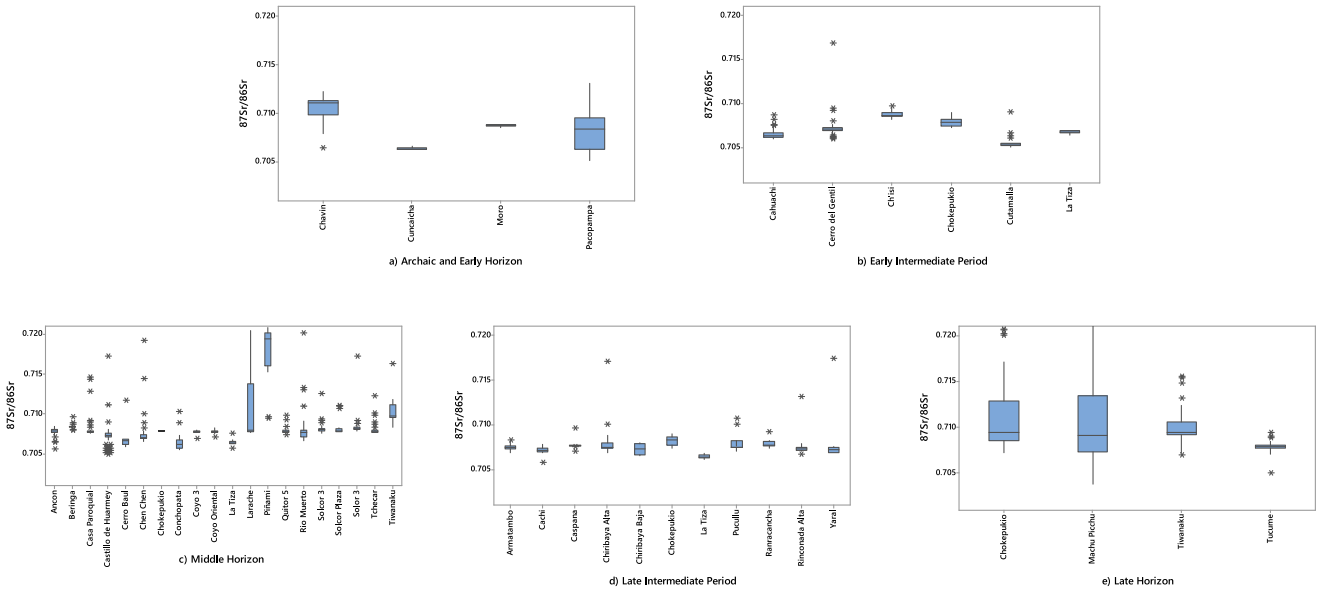

Fig. 5. Boxplots of $^{87}Sr/^{86}Sr$ values by time period.

3.3. Intra-lifetime and sex-based variation in human skeletal samples

Human enamel signatures (s = 0.002, n = 975) are significantly more varied than bone signatures (s = 0.001, n = 377) (F-test statistic = 0.40, $p < 0.0001$) (Fig. 6). Variability between infancy/early childhood-forming enamel samples (s = 0.002, n = 402) and middle childhood samples (s = 0.002, n = 427) was slightly greater than between enamel forming during teen years (s = 0.001, n = 163) and bone forming during late life (s = 0.001, n = 361). Among the developmental categories of tissue types, the two earliest phases showed the greatest variation in $^{87}Sr/^{86}Sr$ values (Bartlett's test statistic = 181.75, $p < 0.001$) (Fig. 6).

$^{87}Sr/^{86}Sr$ enamel variances (reflecting childhood and adolescence) are not significantly different between males (s = 0.002, n = 400) and females (s = 0.002, n = 407) (F test statistic = 0.82, p = 0.05). However, variance in bone $^{87}Sr/^{86}Sr$ is significantly greater for males (s = 0.001, n = 126), than for females (s = 0.0007, n = 178) (F-test statistic = 0.32 $p < 0.0001$).

3.4. $^{87}Sr/^{86}Sr$ isoscape model for the andes

As expected, the archaeological values exhibited significant clustering, showing that similar $^{87}Sr/^{86}Sr$ values are closer to each other than dissimilar ones. Values were spatially autocorrelated (Moran's Index = 0.25, z-score = 53.29, $p < 0.0001$) at the 99% confidence level. Of the 1640 plotted values, there were 94 high-low and low-high clusters identified, including 23 outliers from Machu Picchu and 22 outliers from Larache (Table 4). These values were considered non-representative of local bioavailable strontium signatures and were excluded from the geostatistical model.

Given the similar homogeneity between artifacts, faunal, and human samples as well as between bone and enamel tissues, all remaining non-spatial outlier $^{87}Sr/^{86}Sr$ values (n = 1546) were used to generate the archaeological isoscape model (Fig. 7). The model demonstrates a strong east-west trend with predicted $^{87}Sr/^{86}Sr$ values increasing steadily from 0.70384 near the ocean to 0.70951 and greater on the eastern Andean slopes. The lowest predicted $^{87}Sr/^{86}Sr$ values in the northern Peruvian coast around Trujillo, the Nasca desert, and around mid-Chile near modern Santiago. The highest (most radiogenic) values are in the Bolivian altiplano and the eastern slopes of the Andes into the rainforest. The best-fit model was achieved using the equation: predicted $^{87}Sr/^{86}Sr$ = 0.54361 * (measured $^{87}Sr/^{86}Sr$) + 0.32308.

Cross-validation and model assessment statistics show the archaeological isoscape model is a good fit for the measured $^{87}Sr/^{86}Sr$ values (Table S2). The standard error surface (Fig. 8) was derived from cross-validation process and shows errors between predicted and measured values from 0.0003 to 0.0025. The model mean prediction error is < 0.0001 showing the model predictions are unbiased (Table S2). The nearly-identical average standard error and root-mean-square prediction error shows the model correctly assesses the variability in prediction. The root-mean-square standardized error shows a slight underestimation in the variability of the predictions.

Validation of the test set again shows excellent fit between predictions and measured values, ranging in absolute value of the error from 0.0003 to 0.007 (Table S2 and Table S3). The highest error rates were observed in sites like Larache and Machu Picchu, already noted in the corresponding publications for their small sample sizes, broad $^{87}Sr/^{86}Sr$ ranges, and high percentages of IQR outliers relative to non-outliers.

4. Discussion

Modeling pan-Andean spatial trends in archaeological $^{87}Sr/^{86}Sr$ values through geostatistical methods shows an east-west gradient of less to more radiogenic values (Fig. 7) that enable us to constrain geographic areas of possible provenience for human, faunal, and artifact samples within many known long-distance exchange networks. The entire range of $^{87}Sr/^{86}Sr$ values in archaeological Andean samples (0.7038–0.7234) is just as wide as reported in archaeological and environmental samples globally (Bentley, 2006), so the Andes overall presents sufficient variability to enable strontium isotope sourcing between modeled zones. Among the modeled data points, it is possible that higher variability and the large sample size of migratory fauna inflated the range of variation expected for humans in the model. Most of the faunal values (187/232 = 80.6%) modeled were from large domesticated animals like camelids—common traveling companions for long-distance caravans that often have non-local residential histories (deFrance et al., 2016; Knudson et al., 2012a; Nielsen, 2001; Takigami et al., 2019; Thornton et al., 2011; Tomczyk et al., 2019, contributions in Tripcevich and Capriles, 2016). Nonetheless, the similar variance of the migratory faunal subsample to the human subsample demonstrates that

Table 3
Number and percentage of samples within sites determined to be outside of the interquartile range (n = 1491 samples which could be assigned to a temporal category).

Time	Site	Site n	# samples outside of IQR	% of samples outside of IQR
Pre- Early Intermediate Period = 4 sites n = 90 samples	Chavin	11	1	9.1
	Cuncaicha	13	0	0.0
	Moro	15	0	0.0
	Pacopampa	51	0	0.0
Early Intermediate Period n = 6 sites n = 199 samples	Cahuachi	56	5	8.9
	Cerro del Gentil	81	17	20.0
	Ch'isi	23	1	4.0
	Chokepukio	8	0	0.0
	Cutamalla	22	4	18.2
	La Tiza	9	0	0.0
Middle Horizon n = 20 sites n = 695 samples	Ancon	64	4	6.3
	Beringa	58	6	10.3
	Casa Paroquial	36	7	19.4
	Castillo de Huarmey	87	16	18.4
	Cerro Baul	11	1	9.1
	Chen Chen	66	11	16.7
	Chokepukio	1	NA	NA
	Conchopata	19	2	10.5
	Coyo 3	14	1	7.1
	Coyo Oriental	26	2	7.7
	La Tiza	19	2	10.5
	Larache	37	0	0.0
	Piñami	12	2	16.7
	Quitor 5	29	4	13.8
	Rio Muerto	58	4	6.9
	Solcor 3	50	5	10.0
	Solcor Plaza	16	3	18.8
	Solor 3	20	4	20.0
	Tchecar	59	6	10.2
	Tiwanaku	13	1	7.8
Late Intermediate Period n = 11 sites n = 311 samples	Armatambo	118	1	0.8
	Cachi	14	1	7.1
	Caspana	30	3	10.0
	Chiribaya Alta	36	5	13.9
	Chiribaya Baja	10	0	0.0
	Chokepukio	5	0	0.0
	La Tiza	5	0	0.0
	Pucullu	10	3	30.0
	Ranracancha	10	1	10.0
	Rinconada Alta	60	2	3.3
	Yaral	13	1	7.7
Late Horizon n = 4 sites n = 196 samples	Chokepukio	38	5	13.2
	Machu Picchu	51	0	0.0
	Tiwanaku	48	5	10.4
	Tucume	59	6	10.2

all faunal and human samples can be confidently included for modeling bioavailable strontium in local food webs.

4.1. Highest relative proportions of $^{87}Sr/^{86}Sr$ outliers in the Early Intermediate Period and Middle Horizon

Non-spatial statistics yielded important temporal trends which clarify aspects of population history through time. Using the least conservative measure for defining outliers (IQR), the highest relative proportions of outliers within sites was observed for the EIP (13.9% outliers), Middle Horizon (11.7%), and Late Horizon (10.7%). While pre-EIP and LIP sites show relative proportions of IQR outliers under 10.0%. This finding is consistent with prior research that has characterized the Andean Middle Horizon (Knudson and Torres-Rouff, 2014, 2015) and Late Horizon (Andrushko et al., 2009; Knudson et al., 2012a; Turner et al., 2009) as periods of heightened inter-regional exchange, cultural and biogeographic diversity, and high levels of population mobility. The low relative proportion of outliers in the LIP is also

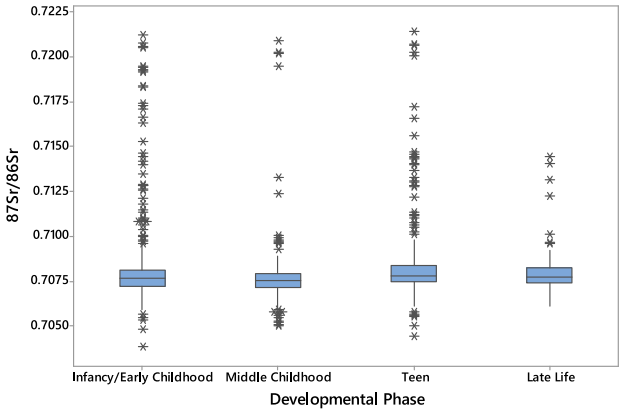

Fig. 6. Enamel and bone $^{87}Sr/^{86}Sr$ values by developmental phase of the tissue.

consistent with the characterization of this period as a time of insularity, conflict, and constrained inter-regional interaction in the face of environmental challenges and Wari imperial dissolution (Arkush, 2018; Arkush, 2011; Bauer and Kellett, 2010; Kurin, 2016; Langlie and Arkush, 2016; Tung et al., 2016).

The high relative proportion of IQR outliers for EIP sites is surprising given evidence for intergroup conflict and resource stress that led to balkanization during this period (Conlee, 2016; Proulx, 1999; Schreiber and Lancho Rojas, 2003; Silverman and Proulx, 2002; Valdez, 2009; Vaughn, 2009). While the relatively constrained IQR ranges of EIP sites might indicate communities were comprised mostly of individuals with residences restricted to those communities, the large proportions of IQR outliers suggests that these EIP communities experienced more immigration than during other time periods. This contrasts with the sites with the largest IQR ranges (Machu Picchu, Chokepukio, Larache Pacopampa), which may have been comprised overall of inhabitants from a wider geographic range, leading to fewer statistical outliers. It is also worth considering that the broader ranges may reflect more heterogeneous strontium isotope catchments, which could be due to heterogeneous bedrock, or to extensive consumption of imported foods, use of fertilizers, or anthropogenic burning at those sites.

4.2. Developmental and sex-based patterns of $^{87}Sr/^{86}Sr$ variability throughout the andes

The highest variability was demonstrated in enamel $^{87}Sr/^{86}Sr$ values

Table 4
Archaeological $^{87}Sr/^{86}Sr$ values excluded from the isoscape model due to being spatial outliers as determined by the Anselin's Local Moran's I test (n = 94 excluded values).

Site	Total Spatial Outliers (Local Anselin Moran's I)
Armatambo	4
Cahuachi	2
Castillo de Huarmey	4
Cerro del Gentil	3
Chavin	1
Chen Chen	11
Chokepukio	13
Conchopata	2
Jauranga	1
La Tiza	1
Larache	22
Machu Picchu	23
Rinconada Alta	1
Solcor 3	1
Tiwanaku	5
Total	94

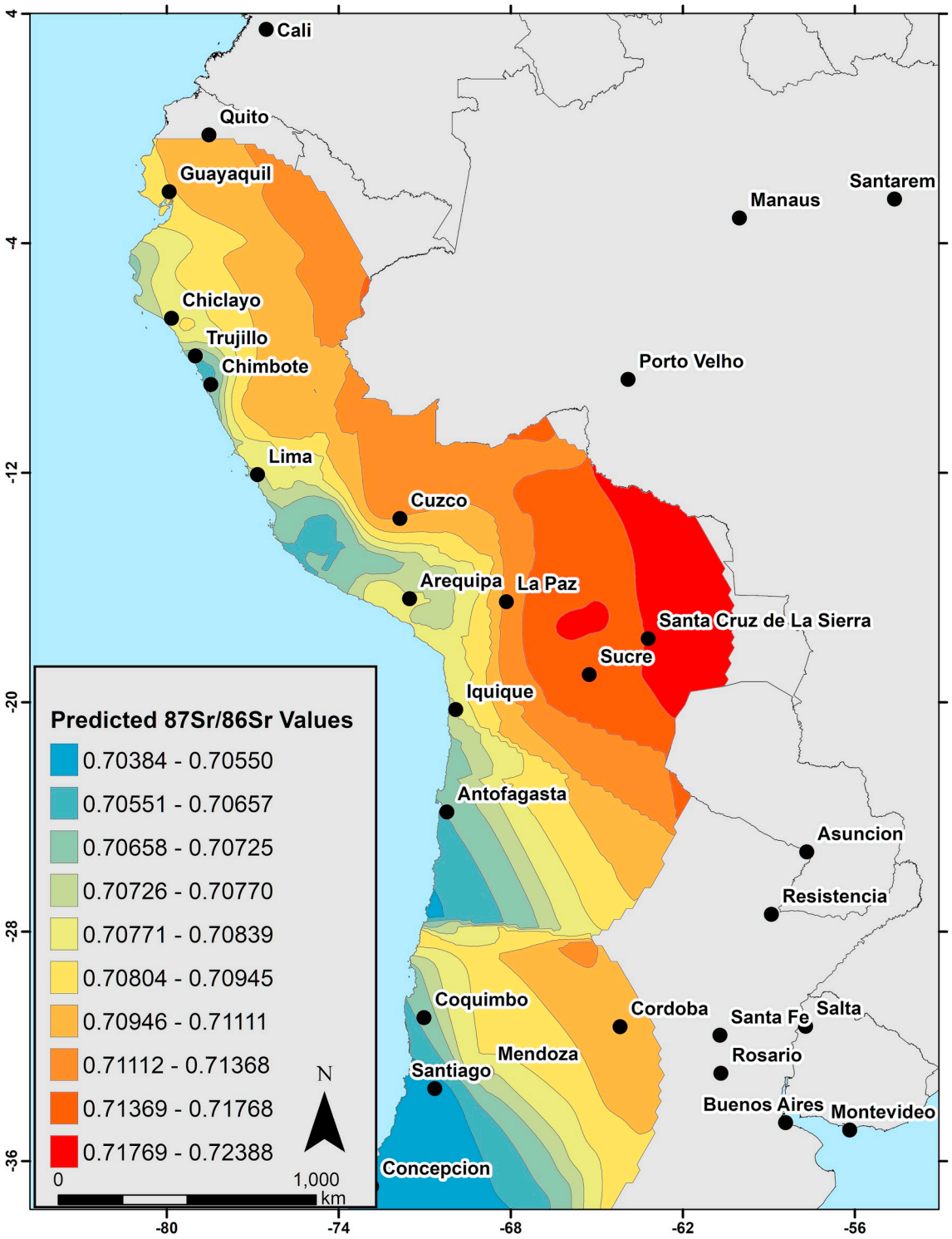

Fig. 7. Predictive $^{87}Sr/^{86}Sr$ isoscape model (isoscape generated in the Albers Equal Area Conic system, but grid references latitude and longitude).

from infancy/early childhood and middle childhood, and that variability ($s = 0.002$) is identical to that of the entire archaeological human sample. This could indicate that infancy and early childhood were important times for familial mobility, as the resource needs of childbearing and childrearing are intensive. Families may have moved frequently during their offspring's early years to leverage different networks of community support, security, and nutritional access. It is also possible that this variability in early-forming enamel reflects diverse dietary sources of strontium during childhood, which would have spanned in utero and breastfeeding contributions from maternal diet, weaning foods, and foods foraged by children (e.g. Greenwald et al., 2016).

Sex-based variability in $^{87}Sr/^{86}Sr$ from enamel was similar, but males across the prehistoric Andes showed higher variability in late-life bone samples than females. This could suggest that childhood mobility and diets across the Andes were similar for boys and girls, but that males were more mobile than females as adults, whether this was due to permanent residential changes or short-term mobility during their last years

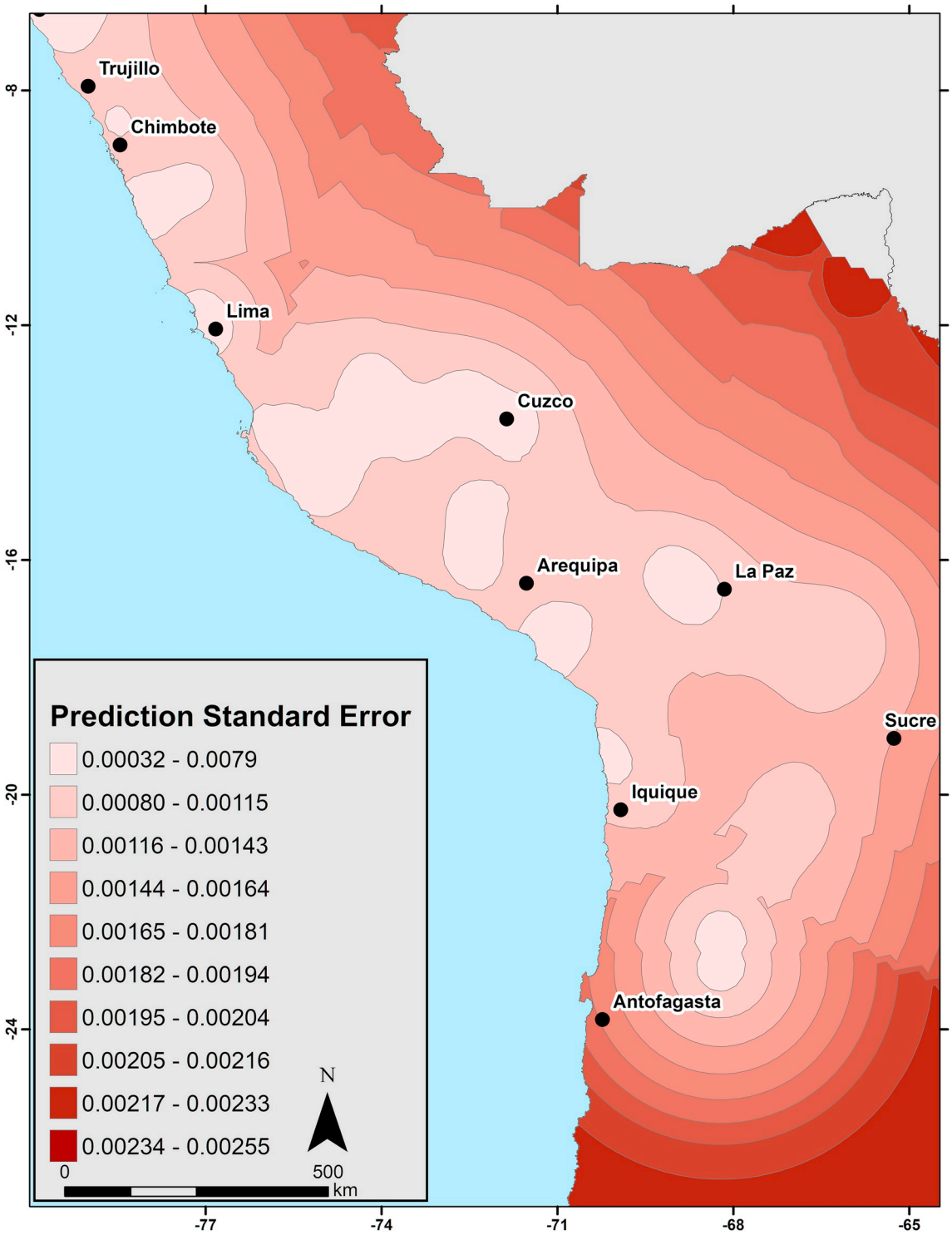

Fig. 8. Prediction standard error map (generated in the Albers Equal Area Conic system, but grid references latitude and longitude).

of life. However, this enhanced variability for males might also reflect that males had greater access to geographically-diverse or imported foods during their adult years, while females consumed higher relative proportions of locally-sourced foods. The exceptionally low standard deviation among late-life bone $^{87}Sr/^{86}Sr$ values for females across the Andes ($s = 0.0007$, $n = 178$) hints that female social roles and subsistence practices were tightly constrained and their mobility largely limited to their natal communities throughout Andean prehistory.

4.3. Equifinality in the andean strontium isotope system

The most serious limitation of the archaeological strontium isoscape is the problem of equifinality, described by Price and colleagues as the overlapping $^{87}Sr/^{86}Sr$ values of geographically-distant regions with similar underlying bedrock age and morphology (Price et al., 2002; Price et al., 2007). The isoscape presented herein predicts, for example, a range of 0.7077–0.7084 throughout much of the Arequipa region, with only limited intrusion of less radiogenic values from highland geological formations. Those ranges are duplicated in central coastal Peru (around

Lima), and in the southern Peruvian portion of Lake Titicaca, so that individuals within this range could have been locals from Arequipa, migrants from distant but geologically-similar parts of Arequipa, or migrants from those distant regions. The model also shows large regions of homogeneity around the southern Nasca region mirroring earlier geological models (Schenk et al., 1999), so that individuals from one limit of that homogeneous region might not be distinguishable from a non-local from a distant, but geologically-similar region (this issue was also observed in Knudson et al., 2009). Therefore, the utility of this single-isotope model depends on the nature of settlement patterns and exchange networks known or suspected to have been in existence—when those cut across isoscape zones, this model can help to geolocate outliers. However, when hypothesized connections are within regions of modeled homogeneity, or between bordering zones with contiguous values, this study shows that multiple isotopic signatures are critical for sourcing samples to likely places of origin.

5. Conclusions

Applying big data approaches to bioarchaeological isotope analysis can yield key insights into spatiotemporal and biological patterns of bioavailable strontium variability. The isoscape model presented clarifies the utility and limitations of a single isotope model for sourcing samples to discrete regions of origin within the Andean strontium isotope system. Given the immense promise of strontium isoscape models for the Andes, it is critical for researchers to publish and share $^{87}Sr/^{86}Sr$ values along with the spatial and temporal contexts of those archaeological and baseline data. This study has demonstrated that strontium isotope variability in the Andes is a spatially-contingent phenomenon, which merits modeling with spatially-explicit geostatistical methods. Collaboration and data sharing with ecologists, geologists, and other non-archaeologists will help more accurately model baseline strontium expectations in this hydrologically and geologically-diverse part of the world.

Finally, this study emphasizes the need for environmental baseline models of the entire food chain in the Andean region. As other researchers have argued (Crowley et al., 2017; Grimstead et al., 2017; Lengfelder et al., 2019), modeling the mixed-source contributions of strontium within local food webs is essential for accurately predicting skeletal isotope values at local, pan-regional, and continental scales. Ongoing research is examining the variability of water, plant, and faunal $^{87}Sr/^{86}Sr$ values throughout southern Peru in order to develop environmental baseline isoscapes for the study region. These models will be tested against the archaeological values compiled by this study in order to understand which materials or combinations thereof provide the best environmental proxies for archaeological tissues throughout the Andes. These models, combined with multifaceted and deeply-contextualized studies of prehistoric subsistence, trade, and mobility patterns, with help to define expected baseline ranges within isotopic catchment areas, and help us move toward probabilistic determination of sample origins within these complex biogeographical networks.

Declaration of interests

The authors declare that they have no known competing financial interests or personal relationships that could have appeared to influence the work reported in this paper.

Acknowledgements

We thank Jake Dean, Camden Hatley, and Kathryn Orr, the Undergraduate Research Apprentices that assisted with data compilation as part of their work for the Andean Paleomobility Unification (APU) Project and the Archaeological Chemistry Laboratory in the Center for Bioarchaeological Research at the School of Human Evolution and Social Change at Arizona State University. We also are very thankful to the following archaeologists, who assisted with locating sites: Matt Biwer, Sarah Marsteller, Christina Torres-Rouff, and Tiffiny Tung. Andrew Zipkin and the anonymous reviewers provided valuable and substantive feedback on the manuscript and are very much appreciated.

Appendix A. Supplementary data

Supplementary data to this article can be found online at https://doi.org/10.1016/j.jas.2020.105121.

Funding

This work was supported by a National Science Foundation SBE Postdoctoral Fellowship to Beth K. Scaffidi [grant number 1809470].

References

Adams, S., Grün, R., McGahan, D., Zhao, J.X., Feng, Y., Nguyen, A., Willmes, M., Quaresimin, M., Lobsey, B., Collard, M., 2019. A strontium isoscape of north-east Australia for human provenance and repatriation. Geoarchaeology 34, 231–251.
Andrushko, V.A., Buzon, M.R., Simonetti, A., Creaser, R.A., 2009. Strontium isotope evidence for prehistoric migration at Chokepukio, Valley of Cuzco, Peru. Lat. Am. Antiq. 20, 57–75.
Arkush, E., 2018. Coalescence and defensive communities: insights from an andean Hillfort town. Camb. Archaeol. J. 28, 1–22.
Arkush, E.N., 2011. Hillforts of the Ancient Andes. University Press of Florida, Gainesville.
Aufderheide, A.C., 1989. Chemical Analysis of Skeletal Remains. Alan R. Liss, New York.
Barberena, R., Durán, V.A., Novellino, P., Winocur, D., Benítez, A., Tessone, A., Quiroga, M.N., Marsh, E.J., Gasco, A., Cortegoso, V., 2017. Scale of human mobility in the southern Andes (Argentina and Chile): a new framework based on strontium isotopes. Am. J. Phys. Anthropol. 164, 305–320.
Bataille, C.P., Bowen, G.J., 2012. Mapping 87 Sr/86 Sr variations in bedrock and water for large scale provenance studies. Chem. Geol. 304, 39–52.
Bataille, C.P., Laffoon, J., Bowen, G.J., 2012. Mapping multiple source effects on the strontium isotopic signatures of ecosystems from the circum-Caribbean region. Ecosphere 3, 1–24.
Bataille, C.P., von Holstein, I.C., Laffoon, J.E., Willmes, M., Liu, X.-M., Davies, G.R., 2018. A bioavailable strontium isoscape for Western Europe: a machine learning approach. PloS One 13, e0197386.
Bauer, B.S., Kellett, L.C., 2010. Cultural transformations of the chanka homeland (andahuaylas, Peru) during the late Intermediate Period (AD 1000–1400). Lat. Am. Antiq. 21, 87–111.
Bentley, R.A., 2006. Strontium isotopes from the earth to the archaeological skeleton: a review. J. Archaeol. Method Theor 13, 135–187.
Bentley, R.A., Price, T.D., Stephan, E., 2004. Determining the 'local'87Sr/86Sr range for archaeological skeletons: a case study from Neolithic Europe. J. Archaeol. Sci. 31, 365–375.
Bethard, J.D., Gaither, C., Sánchez, V.V., Tham, T.R., Kent, J.D., 2008. Isótopos estables, dieta y movilidad de los pobladores de un conjunto residencial en Santa Rita B, Valle de Chao, Perú. Archaeobios 3.
Borić, D., Price, T.D., 2013. Strontium isotopes document greater human mobility at the start of the Balkan Neolithic. Proc. Natl. Acad. Sci. Unit. States Am. 110, 3298–3303.
Bowen, G., 2010. Isoscapes: spatial patterns in isotopic biogeochemistry. Annu. Rev. Earth Planet Sci. 38, 161–187.
Budd, P., Montgomery, J., Barreiro, B., Thomas, R.G., 2000. Differential diagenesis of strontium in archaeological human dental tissues. Appl. Geochem. 15, 687–694.
Buikstra, J.E., Price, T.D., Wright, L.E., Burton, J.A., 2004. Tombs from the Copan acropolis: a life history approach. In: Bell, E.E., Canuto, M.A., Sharer, R. (Eds.), Understanding Early Classic Copan. University of Pennsylvania Museum of Archaeology and Anthropology, Philadephia, pp. 191–212.
Burton, J.H., Hahn, R., 2016. Assessing the "local" 87 Sr/86 Sr ratio for humans. In: Grupe, G., McGlynn, G.C. (Eds.), Isotopic Landscapes in Bioarchaeology. Springer, Berlin, pp. 113–121.
Buzon, M.R., Conlee, C.A., Simonetti, A., Bowen, G.J., 2012. The consequences of Wari contact in the Nasca region during the Middle Horizon: archaeological, skeletal, and isotopic evidence. J. Archaeol. Sci. 39, 2627–2636.
Chala-Aldana, D., Bocherens, H., Miller, C., Moore, K., Hodgins, G., Rademaker, K., 2018. Investigating mobility and highland occupation strategies during the Early Holocene at the Cuncaicha rock shelter through strontium and oxygen isotopes. J. Archaeol. Sci.: Rep. 19, 811–827.
Conlee, C.A., 2016. Beyond the Nasca Lines: Ancient Life at La Tiza in the Peruvian Desert. University Press of Florida, Gainesville.
Conlee, C.A., Buzon, M.R., Gutierrez, A.N., Simonetti, A., Creaser, R.A., 2009. Identifying foreigners versus locals in a burial population from Nasca, Peru: an investigation using strontium isotope analysis. J. Archaeol. Sci. 36, 2755–2764.
Copeland, S.R., Cawthra, H.C., Fisher, E.C., Lee-Thorp, J.A., Cowling, R.M., Le Roux, P.J., Hodgkins, J., Marean, C.W., 2016. Strontium isotope investigation of ungulate movement patterns on the Pleistocene Paleo-Agulhas plain of the Greater Cape floristic region, South Africa. Quat. Sci. Rev. 141, 65–84.
Cressie, N., 1993. Statistics for Spatial Data. John Wiley and Sons, Inc., New York, NY.

Crowley, B.E., Miller, J.H., Bataille, C.P., 2017. Strontium isotopes (87Sr/86Sr) in terrestrial ecological and palaeoecological research: empirical efforts and recent advances in continental-scale models. Biol. Rev. Camb. Phil. Soc. 92, 43–59.
deFrance, S.D., Capriles, J.M., Tripcevich, N., 2016. Pastoralism through time in southern Peru. In: Capriles, J.M., Tripcevich, N. (Eds.), The Archaeology of Andean Pastoralism. University of New Mexico Press, Albuquerque, NM, pp. 119–138.
Durán, V.A., Cortegoso, V., Barberena, R., Frigolé, C., Novellino, P., Lucero, G., Yebra, L., Gasco, A., Winocur, D., Benítez, A., 2018. 'To and fro'the southern Andean highlands (Argentina and Chile): archaeometric insights on geographic vectors of mobility. J. Archaeol. Sci.: Rep. 18, 668–678.
Eriksson, G., Frei, K.M., Howcroft, R., Gummesson, S., Molin, F., Lidén, K., Frei, R., Hallgren, F., 2018. Diet and mobility among Mesolithic hunter-gatherers in Motala (Sweden)-the isotope perspective. J. Archaeol. Sci.: Rep. 17, 904–918.
Estevan, R., Martínez-Castro, D., Suarez, L., Moya, A., Silva, Y., 2019. First Two and a Half Years of Aerosol Measurements with an AERONET Sunphotometer at the Huancayo Observatory, Peru. Atmospheric Environment, p. 100037. X.
Evans, J., Pearson, M.P., Madgwick, R., Sloane, H., Albarella, U., 2019. Strontium and oxygen isotope evidence for the origin and movement of cattle at Late Neolithic Durrington Walls, UK. Archaeol. Anthropol. Sci. 1–17.
Evans, J.A., Chenery, C.A., Fitzpatrick, A.P., 2006. Bronze Age childhood migration of individuals near Stonehenge, revealed by strontium and oxygen isotope tooth enamel analysis. Archaeometry 48, 309–321.
Evans, J.A., Tatham, S., 2004. Defining 'local Signature'in Terms of Sr Isotope Composition Using a Tenth-To Twelfth-Century Anglo-Saxon Population Living on a Jurassic Clay-Carbonate Terrain, vol. 232. Geological Society, London, Special Publications, Rutland, UK, pp. 237–248.
Fahy, G.E., Deter, C., Pitfield, R., Miszkiewicz, J.J., Mahoney, P., 2017. Bone deep: variation in stable isotope ratios and histomorphometric measurements of bone remodelling within adult humans. J. Archaeol. Sci. 87, 10–16.
Faure, G., Mensing, T.M., 2005. Isotopes: Principles and Applications. John Wiley & Sons, Hoboken, NJ.
Fenner, J.N., Frost, C.D., 2009. Modern Wyoming plant and pronghorn isoscapes and their implications for archaeology. J. Geochem. Explor. 102, 149–156.
Fenner, J.N., Wright, L.E., 2014. Revisiting the strontium contribution of sea salt in the human diet. J. Archaeol. Sci. 44, 99–103.
Fisher, E.C., Bar-Matthews, M., Jerardino, A., Marean, C.W., 2010. Middle and Late Pleistocene paleoscape modeling along the southern coast of South Africa. Quat. Sci. Rev. 29, 1382–1398.
Frei, K.M., Frei, R., 2011. The geographic distribution of strontium isotopes in Danish surface waters–A base for provenance studies in archaeology, hydrology and agriculture. Appl. Geochem. 26, 326–340.
Frei, K.M., Price, T.D., 2012. Strontium isotopes and human mobility in prehistoric Denmark. Archaeol. Anthropol. Sci. 4, 103–114.
Frei, R., Frei, K.M., 2013. The geographic distribution of Sr isotopes from surface waters and soil extracts over the island of Bornholm (Denmark)–A base for provenance studies in archaeology and agriculture. Appl. Geochem. 38, 147–160.
Graustein, W.C., 1989. 87Sr/86Sr Ratios Measure the Sources and Flow of Strontium in Terrestrial Ecosystems, Stable Isotopes in Ecological Research. Springer, pp. 491–512.
Greenwald, A.M., Eerkens, J.W., Bartelink, E.J., 2016. Stable isotope evidence of juvenile foraging in prehistoric Central California. J. Archaeol. Sci.: Rep. 7, 146–154.
Grimstead, D., Clark, A., Rezac, A., 2018. Uranium and vanadium concentrations as a trace element method for identifying diagenetically altered bone in the inorganic phase. J. Archaeol. Method Theor 25, 689–704.
Grimstead, D.N., Nugent, S., Whipple, J., 2017. Why a standardization of strontium isotope baseline environmental data is needed and recommendations for methodology. Adv. Archaeol. Pract. 5, 184–195.
Grupe, G., Hölzl, S., Kocsis, B., Kröger, P., Mauder, M., Mayr, C., Ntoutsi, E., Scmahl, W., Söllner, A.T., Wycisk, D., 2017. Isotopic mapping and migration research based on bioarchaeological finds. In: Scholz, A., Bartleheim, M., Hardenberg, R., Staecker, J. (Eds.), ResourceCultures: Sociocultural Dynamics and the Use of Resources - Theories, Methods, and Perspectives. University of Tübingen, Tübingen, p. 195.
Hedges, R.E., 2002. Bone diagenesis: an overview of processes. Archaeometry 44, 319–328.
Hedman, K.M., Slater, P.A., Fort, M.A., Emerson, T.E., Lambert, J.M., 2018. Expanding the strontium isoscape for the American midcontinent: identifying potential places of origin for Cahokian and Pre-Columbian migrants. J. Archaeol. Sci.: Rep. 22, 202–213.
Hewitt, B.R., 2013. Foreigners Among the Dead at Túcume, Peru: Assesssing Residential Mobility Using Isotopic Tracers. PhD Dissertation), University of Western Ontario, Ontario.
Hillson, S., 1996. Dental Anthropology. Cambridge University Press, Cambridge England ; New York.
Hillson, S., 1986. Teeth. Cambridge University Press, Cambridge.
Hodell, D.A., Quinn, R.L., Brenner, M., Kamenov, G., 2004. Spatial variation of strontium isotopes (87Sr/86Sr) in the Maya region: a tool for tracking ancient human migration. J. Archaeol. Sci. 31, 585–601.
Hrnčíř, V., Laffoon, J.E., 2019. Childhood Mobility Revealed by Strontium Isotope Analysis: a Review of the Multiple Tooth Sampling Approach. Archaeological and Anthropological Sciences.
Johnston, K., Ver Hoef, J.M., Krivoruchko, K., Lucas, N., 2001. Using ArcGIS Geostatistical Analyst. Esri Redlands, Redlands, CA.
Juengst, S.L., 2017. 3 inclusive communities in the Titicaca basin during the early Horizon. Archeol. Pap. Am. Anthropol. Assoc. 28 (1), 24–37.
Juengst, S.L., Chávez, S.J., Hutchinson, D.L., Mohr Chávez, K., 2015. Trauma in the Titicaca basin, Bolivia (AD 1000-1450). Int. J. Osteoarchaeol.
Kamenov, G., Macfarlane, A.W., Riciputi, L., 2002. Sources of lead in the San Cristobal, Pulacayo, and Potosi mining districts, Bolivia, and a reevaluation of regional ore lead isotope provinces. Econ. Geol. 97, 573–592.
Kamenov, G.D., Brenner, M., Tucker, J.L., 2009. Anthropogenic versus natural control on trace element and Sr–Nd–Pb isotope stratigraphy in peat sediments of southeast Florida (USA),~ 1500 AD to present. Geochem. Cosmochim. Acta 73, 3549–3567.
Kamenov, G.D., Lofaro, E.M., Goad, G., Krigbaum, J., 2018. Trace elements in modern and archaeological human teeth: implications for human metal exposure and enamel diagenetic changes. J. Archaeol. Sci. 99, 27–34.
Klerkx, J., Deutsch, S., Pichler, H., Zeil, W., 1977. Strontium isotopic composition and trace element data bearing on the origin of Cenozoic volcanic rocks of the central and southern Andes. J. Volcanol. Geoth. Res. 2, 49–71.
Knudson, K.J., 2008. Tiwanaku influence in the south central Andes: strontium isotope analysis and Middle Horizon migration. Lat. Am. Antiq. 3–23.
Knudson, K.J., Buikstra, J.E., 2007. Residential mobility and resource use in the Chiribaya polity of southern Peru: strontium isotope analysis of archaeological tooth enamel and bone. Int. J. Osteoarchaeol. 17, 563–580.
Knudson, K.J., Gardella, K.R., Yaeger, J., 2012a. Provisioning Inka feasts at Tiwanaku, Bolivia: the geographic origins of camelids in the Pumapunku complex. J. Archaeol. Sci. 39, 479–491.
Knudson, K.J., Giersz, M., Więckowski, W., Tomczyk, W., 2017. Reconstructing the lives of Wari elites: paleomobility and paleodiet at the archaeological site of Castillo de Huarmey, Peru. J. Archaeol. Sci.: Rep. 13, 249–264.
Knudson, K.J., O'Donnabhain, B., Carver, C., Cleland, R., Price, T.D., 2012b. Migration and viking dublin: paleomobility and paleodiet through isotopic analyses. J. Archaeol. Sci. 39, 308–320.
Knudson, K.J., Pestle, W.J., Torres-Rouff, C., Pimentel, G., 2012c. Assessing the life history of an andean traveller through biogeochemistry: stable and radiogenic isotope analyses of archaeological human remains from Northern Chile. Int. J. Osteoarchaeol. 22, 435–451.
Knudson, K.J., Price, T.D., 2007. Utility of multiple chemical techniques in archaeological residential mobility studies: case studies from Tiwanaku-and Chiribaya-affiliated sites in the Andes. Am. J. Phys. Anthropol. 132, 25–39.
Knudson, K.J., Price, T.D., Buikstra, J.E., Blom, D.E., 2004. The use of strontium isotope analysis to investigate Tiwanaku migration and mortuary ritual in Bolivia and Peru. Archaeometry 46, 5–18.
Knudson, K.J., Stanish, C., Cerna, M.C.L., Faull, K.M., Tantaleán, H., 2016. Intra-individual variability and strontium isotope measurements: a methodological study using 87 Sr/86 Sr data from Pampa de los Gentiles, Chincha Valley, Peru. J. Archaeol. Sci.: Rep. 5, 590–597.
Knudson, K.J., Torres-Rouff, C., 2014. Cultural diversity and paleomobility in the andean middle Horizon: radiogenic strontium isotope analyses in the san Pedro de Atacama oases of northern Chile. Lat. Am. Antiq. 25, 170–188.
Knudson, K.J., Torres-Rouff, C., 2015. Migration as a response to environmental and political disruption. In: Baker, B., Tsuda, T. (Eds.), Migration and Disruptions: toward a Unifying Theory of Ancient and Contemporary Migrations. University Press of Florida, Gainesville, FL, pp. 123–141.
Knudson, K.J., Torres-Rouff, C., 2009. Investigating cultural heterogeneity in San Pedro de Atacama, northern Chile, through biogeochemistry and bioarchaeology. Am. J. Phys. Anthropol. 138, 473–485.
Knudson, K.J., Tung, T.A., 2011. Investigating regional mobility in the southern hinterland of the Wari Empire: biogeochemistry at the site of Beringa, Peru. Am. J. Phys. Anthropol. 145, 299–310.
Knudson, K.J., Tung, T.A., 2007. Using Archaeological Chemistry to Investigate the Geographic Origins of Trophy Heads in the Central Andes: Strontium Isotope Analysis at the Wari Site of Conchopata, Archaeological Chemistry: Analytical Techniques and Archaeological Interpretation. American Chemical Society, Washington, D.C., pp. 99–113
Knudson, K.J., Tung, T.A., Nystrom, K.C., Price, T.D., Fullagar, P.D., 2005. The origin of the Juch'uypampa Cave mummies: strontium isotope analysis of archaeological human remains from Bolivia. J. Archaeol. Sci. 32, 903–913.
Knudson, K.J., Webb, E., White, C., Longstaffe, F.J., 2014. Baseline data for Andean paleomobility research: a radiogenic strontium isotope study of modern Peruvian agricultural soils. Archaeol. Anthropol. Sci. 6, 205–219.
Knudson, K.J., Williams, S.R., Osborn, R., Forgey, K., Williams, P.R., 2009. The geographic origins of Nasca trophy heads using strontium, oxygen, and carbon isotope data. J. Anthropol. Archaeol. 28, 244–257.
Kootker, L., van Lanen, R., Groenewoudt, B., Altena, E., Panhuysen, R., Jansma, E., Kars, H., Davies, G., 2019. Beyond isolation: understanding past human-population variability in the Dutch town of Oldenzaal through the origin of its inhabitants and its infrastructural connections. Archaeol. Anthropol. Sci. 11, 755–775.
Kootker, L.M., van Lanen, R.J., Kars, H., Davies, G.R., 2016. Strontium isoscapes in The Netherlands: spatial variations in 87 Sr/86 Sr as a proxy for palaeomobility. J. Archaeol. Sci.: Rep. 6, 1–13.
Kurin, D.S., 2016. The Bioarchaeology of Societal Collapse and Regeneration in Ancient Peru. Springer, Cham.
Kurin, D.S., Lofaro, E., Gómez Choque, D., Krigbaum, J., 2016. A bioarchaeological and biogeochemical study of warfare and mobility in Andahuaylas, Peru (ca. AD 1160–1260). Int. J. Osteoarchaeol. 26, 93–103.
Laffoon, J., Espersen, R., Mickleburgh, H., 2018. The life history of an enslaved African: multiple isotope evidence for forced childhood migration from Africa to the Caribbean and associated dietary change. Archaeometry 60, 350–365.
Laffoon, J.E., Hoogland, M.L., 2012. Migration and mobility in the circum-Caribbean: integrating archaeology and isotopic analysis. In: Kaiser, E., Burger, J., Schier, W. (Eds.), Population Dynamics in Prehistory and Early History: New Approaches Using Stable Isotopes and Genetics. De Gruyter, Berlin, Boston, pp. 337–353.

Laffoon, J.E., Sonnemann, T.F., Shafie, T., Hofman, C.L., Brandes, U., Davies, G.R., 2017. Investigating human geographic origins using dual-isotope (87Sr/86Sr, δ18O) assignment approaches. PloS One 12, e0172562.
Langlie, B.S., Arkush, E.N., 2016. Managing mayhem: conflict, environment, and subsistence in the andean late Intermediate Period, puno, Peru. In: VanDerwarker, A. M., Wilson, G.D. (Eds.), The Archaeology of Food and Warfare. Springer, Cham, pp. 259–289.
Larsen, C.S., 2018. Bioarchaeology in perspective: from classifications of the dead to conditions of the living. Am. J. Phys. Anthropol. 165, 865–878.
Lengfelder, F., Grupe, G., Stallauer, A., Huth, R., Söllner, F., 2019. Modelling strontium isotopes in past biospheres–Assessment of bioavailable 87Sr/86Sr ratios in local archaeological vertebrates based on environmental signatures. Sci. Total Environ. 648, 236–252.
Lofaro, E.M., Kurin, D.S., Choque, D.E.G., Krigbaum, J., 2019. Reconstructing diet and mobility using multi-isotopic analysis in Apurimac, Peru (~ AD 880–1260). J. Archaeol. Anthropol. Sci. 11, 1089–1105.
Lucas, C.A., 2012. People on the Move: Examining Tiwanaku State Expansion in the Cochabamba Valley through Strontium Isotope Analysis. Northern Arizona University, Flagstaff, AZ (MA MA Thesis).
Macfarlane, A.W., Marcet, P., LeHuray, A.P., Petersen, U., 1990. Lead isotope provinces of the Central Andes inferred from ores and crustal rocks. Econ. Geol. 85, 1857–1880.
Mader, C., Hölzl, S., Heck, K., Reindel, M., Isla, J., 2018. The llama's share: highland origins of camelids during the late paracas period (370 to 200 BCE) in south peru demonstrated by strontium isotope analysis. J. Archaeol. Sci.: Rep. 20, 257–270.
Mamani, M., Tassara, A., Wörner, G., 2008. Composition and structural control of crustal domains in the central Andes. G-cubed 9.
Marsteller, S.J., Knudson, K.J., Gordon, G., Anbar, A., 2017. Biogeochemical reconstructions of life histories as a method to assess regional interactions: stable oxygen and radiogenic strontium isotopes and Late Intermediate Period mobility on the Central Peruvian Coast. J. Archaeol. Sci.: Rep. 13, 535–546.
Maurer, A.-F., Galer, S.J., Knipper, C., Beierlein, L., Nunn, E.V., Peters, D., Tütken, T., Alt, K.W., Schöne, B.R., 2012. Bioavailable 87Sr/86Sr in different environmental samples—effects of anthropogenic contamination and implications for isoscapes in past migration studies. Sci. Total Environ. 433, 216–229.
Mbeki, L., Kootker, L.M., Kars, H., Davies, G.R., 2017. Sickly slaves, soldiers and sailors. Contextualising the Cape's 18th–19th century Green Point burials through isotope investigation. J. Archaeol. Sci.: Rep. 11, 480–490.
Meiggs, D.C., Arbuckle, B.S., Öztan, A., 2017. The Pixelated Shepherd: Identifying Detailed Local Land-Use Practices at Chalcolithic Köşk Höyük, Central Turkey, Using a Strontium Isotope (87Sr/86Sr) Isoscape, Isotopic Investigations of Pastoralism in Prehistory. Routledge, pp. 77–95.
Montgomery, J., 2010. Passports from the past: investigating human dispersals using strontium isotope analysis of tooth enamel. Ann. Hum. Biol. 37, 325–346.
Nado, K.L., Marsteller, S.J., King, L.M., Daverman, B.M., Torres-Rouff, C., Knudson, K.J., 2012. Examining local social identities through patterns of biological and cultural variation in the Solcor ayllu, San Pedro de Atacama, Chile, Chungara. Revista de Antropología Chilena 44, 341–357.
Nielsen, A., 2001. Ethnoarchaeological perspectives on caravan trade in the South-Central Andes. In: Kuznar, L.A. (Ed.), Ethnoarchaeology of Andean South America: Contributions to Archaeological Method and tTheory, International Monographs in Prehistory. M.I., Ann Arbor, pp. 163–201.
Oliver, M., Webster, R., 2014. A tutorial guide to geostatistics: computing and modelling variograms and kriging. Catena 113, 56–69.
Oliver, M.A., Webster, R., 2015. Basic Steps in Geostatistics: the Variogram and Kriging. Springer Nature, Cham, Switzerland.
Oliver, M.A., Webster, R., 1990. Kriging: a method of interpolation for geographical information systems. Int. J. Geogr. Inf. Syst. 4, 313–332.
Pellegrini, M., Pouncett, J., Jay, M., Pearson, M.P., Richards, M.P., 2016. Tooth enamel oxygen "isoscapes" show a high degree of human mobility in prehistoric Britain. Sci. Rep. 6, 34986.
Perry, M.A., Jennings, C., Coleman, D.S., 2017. Strontium isotope evidence for long-distance immigration into the Byzantine port city of Aila, modern Aqaba, Jordan. Archaeol. Anthropol. Sci. 9, 943–964.
Price, T.D., Blitz, J., Burton, J., Ezzo, J.A., 1992. Diagenesis in prehistoric bone: problems and solutions. J. Archaeol. Sci. 19, 513–529.
Price, T.D., Burton, J.H., Bentley, R.A., 2002. The characterization of biologically available strontium isotope ratios for the study of prehistoric migration. Archaeometry 44, 117–135.
Price, T.D., Burton, J.H., Fullagar, P.D., Wright, L.E., Buikstra, J.E., Tiesler, V., 2015. Strontium Isotopes and the Study of Human Mobility Among the Ancient Maya, Archaeology and Bioarchaeology of Population Movement Among the Prehispanic Maya. Springer, pp. 119–132.
Price, T.D., Burton, J.H., Stoltman, J.B., 2007. Place of origin of prehistoric inhabitants of Aztalan, Jefferson Co., Wisconsin. Am. Antiq. 72, 524–538.
Price, T.D., Johnson, C.M., Ezzo, J.A., Ericson, J., Burton, J.H., 1994. Residential mobility in the prehistoric southwest United States: a preliminary study using strontium isotope analysis. J. Archaeol. Sci. 21, 315–330.
Proulx, D., 1999. Nasca headhunting and the ritual use of trophy heads. In: Rickenbach, J. (Ed.), Nasca: geheimnisvolle zeichen im alten Peru. Museum Rietberg Zurich, Zurich, pp. 79–87.
Pulgar Vidal, J., 1981. Geografía del Perú: Las Ocho Regiones Naturales del Perú, 8a ed. PUCP- Fondo Editorial, Lima, Peru.
Rasmussen, K.L., Milner, G., Skytte, L., Lynnerup, N., Thomsen, J.L., Boldsen, J.L., 2019. Mapping diagenesis in archaeological human bones. Herit. Sci. 7, 41.
Rowe, J.H., Menzel, D., 1967. Peruvian Archaeology: Selected Readings. Peek Publications, Palo Alto, CA.
Schenk, C.J., Viger, R.J., Anderson, C.P., 1999. Maps showing geology, oil and gas fields, and geological provinces of South America. In: Survey, U.S.G. (Ed.), Open-File Report. World Energy Project.
Schreiber, K., Lancho Rojas, J., 2003. Irrigation and Society in the Peruvian Desert: the Puquios of Nasca. Lexington Books, Lanham, MD.
Schwarcz, H.P., White, C.D., Longstaffe, F.J., 2010. Stable and radiogenic isotopes in biological archaeology: some applications. In: West, B.J., Bowen, J.G., Dawson, E.T., Tu, P.K. (Eds.), Isoscapes: Understanding Movement, Pattern, and Process on Earth through Isotope Mapping. Springer Netherlands, Dordrecht, pp. 335–356.
Shand, P., Darbyshire, D., Love, A., Edmunds, W., 2009. Sr isotopes in natural waters: applications to source characterisation and water–rock interaction in contrasting landscapes. Appl. Geochem. 24, 574–586.
Sillen, A., Hall, G., Richardson, S., Armstrong, R., 1998. 87Sr/86Sr ratios in modern and fossil food-webs of the Sterkfontein Valley: implications for early hominid habitat preference. Geochem. Cosmochim. Acta 62, 2463–2473.
Silverman, H., Proulx, D.A., 2002. The Nasca. Blackwell, Malden, Mass; Oxford.
Slovak, N.M., Paytan, A., 2011. Applications of Sr isotopes in archaeology. In: Baskaran, M. (Ed.), Handbook of Environmental Isotope Geochemistry. Springer-Verlag, Berlin, pp. 743–768.
Slovak, N.M., Paytan, A., Rick, J.W., Chien, C.-T., 2018. Establishing radiogenic strontium isotope signatures for Chavín de Huántar, Peru. J. Archaeol. Sci.: Rep. 19, 411–419.
Slovak, N.M., Paytan, A., Wiegand, B.A., 2009. Reconstructing Middle Horizon mobility patterns on the coast of Peru through strontium isotope analysis. J. Archaeol. Sci. 36, 157–165.
Standen, V.G., Santoro, C.M., Arriaza, B., Coleman, D., 2018. Hunting, gathering, and fishing on the coast of the Atacama Desert: chinchorro population mobility patterns inferred from strontium Isotopes. Geoarchaeology 33, 162–176.
Stanish, C., Tantaleán, H., Knudson, K., 2018. Feasting and the evolution of cooperative social organizations circa 2300 BP in Paracas culture, southern Peru. Proc. Natl. Acad. Sci. Unit. States Am. 115, E6716–E6721.
Stojanowski, C.M., Knudson, K.J., 2011. Biogeochemical inferences of mobility of early holocene Fisher-foragers from the southern sahara desert. Am. J. Phys. Anthropol. 146, 49–61.
Swenson, E., Roddick, A., 2018. Constructions of Time and History in the Pre-columbian Andes. University Press of Colorado.
Tachikawa, T., Hato, M., Kaku, M., Iwasaki, A., 2011. Characteristics of ASTER GDEM Version 2, Geoscience and Remote Sensing Symposium (IGARSS), 2011. IEEE International, IEEE, pp. 3657–3660.
Takigami, M., Uzawa, K., Seki, Y., Chocano, D.M., Yoneda, M., 2019. Isotopic evidence for camelid husbandry during the formative period at the Pacopampa site, Peru. Environ. Archaeol. 1–17.
Taylor, D.A., 2002. Dust in the wind. Environ. Health Perspect. 110, A80–A87.
Thomsen, E., Andreasen, R., 2019. Agricultural lime disturbs natural strontium isotope variations: implications for provenance and migration studies. Sci. Adv. 5, 1–11.
Thornton, E.K., Defrance, S.D., Krigbaum, J., Williams, P.R., 2011. Isotopic evidence for middle Horizon to 16th century camelid herding in the osmore valley, Peru. Int. J. Osteoarchaeol. 21, 544–567.
Tomczyk, W., Giersz, M., Sołtysiak, A., Kamenov, G., Krigbaum, J., 2019. Patterns of camelid management in Wari Empire reconstructed using multiple stable isotope analysis: evidence from Castillo de Huarmey, northern coast of Peru. Archaeol. Anthropol. Sci. 11, 1307–1324.
Torres-Rouff, C., Knudson, K.J., 2007. Examining the Life History of an Individual from Solcor 3, San Pedro De Atacama: Combining Bioarchaeology and Archaeological Chemistry, pp. 235–257. Chungara.
Torres-Rouff, C., Knudson, K.J., 2017. Integrating Identities: an innovative bioarchaeological and biogeochemical approach to analyzing the multiplicity of identities in the mortuary record. Curr. Anthropol. 58, 381–409.
Torres-Rouff, C., Knudson, K.J., Pestle, W.J., Stovel, E.M., 2015. Tiwanaku influence and social inequality: a bioarchaeological, biogeochemical, and contextual analysis of the Larache cemetery, San Pedro de Atacama, Northern Chile. Am. J. Phys. Anthropol. 158, 592–606.
Tripcevich, N., Capriles, J.M., 2016. The Archaeology of Andean Pastoralism. University of New Mexico Press, Albuquerque, New Mexico.
Tung, T.A., 2008. Life on the move: bioarchaeological contributions to the study of migration and diaspora communities in the Andes. In: Silverman, H., Isbell, W.H. (Eds.), The Handbook of South American Archaeology. Springer, New York, NY, pp. 671–680.
Tung, T.A., Knudson, K.J., 2008. Social identities and geographical origins of Wari trophy heads from Conchopata, Peru. Curr. Anthropol. 49, 915–925.
Tung, T.A., Miller, M., DeSantis, L., Sharp, E.A., Kelly, J., 2016. Patterns of violence and diet among children during a time of imperial decline and climate change in the ancient Peruvian Andes. In: VanDerwarker, A.M., Wilson, G.D. (Eds.), The Archaeology of Food and Warfare: Food Insecurity in Prehistory, first ed. Springer International Publishing, Cham, pp. 193–228.
Turner, B.L., Kamenov, G.D., Kingston, J.D., Armelagos, G.J., 2009. Insights into immigration and social class at Macchu Picchu, Peru, based on oxygen, strontium, and lead isotopic analysis. J. Archaeol. Sci. 36, 317–332.
Valdez, L.M., 2009. Walled settlements, buffer zones, and human decapitation in the Acari Valley, Peru. J. Anthropol. Res. 65, 389–416.
Valentine, B., Kamenov, G.D., Krigbaum, J., 2008. Reconstructing Neolithic groups in Sarawak, Malaysia through lead and strontium isotope analysis. J. Archaeol. Sci. 35, 1463–1473.

Vaughn, K.J., 2009. The Ancient Andean Village: Marcaya in Prehispanic Nasca. University of Arizona Press, Tucson.
Webb, E.C., 2010. Residential Mobility, Palaeodiet, and Stress in Nasca, Peru: Biogeochemical and Biomolecular Analyses of Achaeological Tissues. The University of Western Ontario, Ontario. Ph.D. Dissertation Dissertation.
Whipkey, C., Capo, R., Chadwick, O., Stewart, B., 2000. The importance of sea spray to the cation budget of a coastal Hawaiian soil: a strontium isotope approach. Chem. Geol. 168, 37–48.
Willmes, M., Bataille, C.P., James, H.F., Moffat, I., McMorrow, L., Kinsley, L., Armstrong, R.A., Eggins, S., Grün, R., 2018. Mapping of bioavailable strontium isotope ratios in France for archaeological provenance studies. Appl. Geochem. 90, 75–86.
Wright, L., 2005. Identifying immigrants to Tikal, Guatemala: defining local variability in strontium isotope ratios of human tooth enamel. J. Archaeol. Sci. 32, 555–566.
Wylde, M., 2017. The Inca Dogs and Their Ancestors. (PhD Thesis). University of Florida, Gainseville, FL.